

Evidence of subsurface control on the coevolution of hillslope morphology and runoff generation

David G. Litwin^{1,2}, Ciaran J. Harman^{2,3}

¹Earth Surface Process Modelling, Helmholtz Center GFZ Potsdam, Potsdam, DE

²Department of Environmental Health and Engineering, Johns Hopkins University, Baltimore, MD, USA

³Department of Earth and Planetary Science, Johns Hopkins University, Baltimore, MD, USA

Key Points:

- We test theoretical predictions about the relationship between hillslope length and relief, saturated area, and transmissivity
- Comparing two watersheds, we find lower transmissivity is associated with shorter hillslopes and larger variably saturated areas
- Hydrogeomorphic modelling suggests that subsurface properties drive the coevolution of differences between the sites

Corresponding author: David G. Litwin, david.litwin@gfz-potsdam.de

Abstract

Topography is a key control on runoff generation, as topographic slope affects hydraulic gradients and curvature affects water flow paths. Simultaneously, runoff generation shapes topography through erosion, affecting landscape morphology over long timescales. Previous modeling efforts suggest that subsurface hydrological properties, relative to climate, are key mediators of this relationship. Specifically, when subsurface transmissivity and water storage capacity are low, (1) saturated areas and storm runoff should be larger and more variable, and (2) hillslopes shorter and with less relief, assuming other geomorphic factors are held constant. However, it remains uncertain whether subsurface properties can exert such strong controls on emergent properties in real landscapes. We compared emergent hydrological function and topography in two watersheds with very similar climatic and geologic history, but very different subsurface properties due to contrasting bedrock lithology. We found that hillslopes were systematically shorter and saturated areas more dynamic at the lower transmissivity site. To test whether these features could be the result of coevolution between topography, hydrological function, and subsurface properties, we estimated all parameters of a coupled groundwater-landscape evolution model for each site. Limitations were revealed in the model’s ability to reproduce aspects of morphology and hydrologic behavior, however, model results suggested differences in drainage density and variably saturated area between the sites could be explained by differences in subsurface properties, and not by differences in geomorphic process rates alone. This work demonstrates one way subsurface hydrology can profoundly affect landscape evolution.

Plain Language Summary

In many humid landscapes, runoff is generated by water that flows through the shallow subsurface from ridges to valleys, eventually emerging and draining to rivers. When subsurface capacity to move water is greater, more water can be transported downslope before surface runoff begins. Surface water may cause erosion, which shapes topography over millions of years. We previously developed a computer model based on these principles and showed that subsurface capacity to store and transmit water affects both runoff generation and topographic evolution. Lower capacity results in more extensive surface runoff and shorter hillslopes, when all other factors are held constant. Here we tested this by comparing two watersheds that differ primarily in their bedrock composition, which affects subsurface water storage and transmissivity. We found that the low transmissivity site experienced more widespread surface runoff in response to precipitation, and had shorter hillslopes, supporting our predictions. We set up computer models for both sites, which suggested that subsurface differences are necessary to explain observed differences in runoff and topography. Finally, we discuss some key limitations of the model that could be improved upon in future attempts to understand how hydrology affects the long-term evolution of Earth’s surface.

1 Introduction

1.1 Background

It has long been understood that there is a close, two-way connection between runoff and the topographic form of landscapes. Topography influences surface and subsurface water flow paths and supplies the elevation component of hydraulic head, while erosion by water shapes landscapes over long timescales. Horton (1945) suggested that there is something valuable to learn about how places work hydrologically by considering this coupling. In particular, such coevolution may be useful for understanding and predicting catchment hydrological function (Troch et al., 2015).

Unfortunately, the vastly different timescales of runoff and evolution of channel networks via erosion has made it challenging to study the coevolution of hydrological and geomorphic states and fluxes. Hydrologists studying runoff generation usually assume that landscape form is fixed, while geomorphologists studying landscape evolution usually assume hydrology can be reduced to a few parameters that capture how hydroclimate affects the efficiency of bedrock erosion and sediment transport.

However, recent advances in modeling and the availability of high performance computers have made it possible to couple hydrologic and geomorphic models, and examine the evolution of hydrologic and geomorphic states together. Litwin et al. (2022) used a shallow aquifer model to generate saturation excess runoff from steady recharge, and used the runoff to drive fluvial incision in a streampower-plus-diffusion landscape evolution model, called DupuitLEM. Litwin et al. (2024) extended DupuitLEM to examine the emergence of variable source area hydrology by adding stochastic precipitation and a simple representation of the vadose zone, thus capturing more realistic hydrologic dynamics.

According to that model subsurface thickness and permeability are important controls on runoff, and consequently, the degree of drainage dissection and length of hillslopes (Figure 1). Subsurface structure in DupuitLEM is represented by a single layer of constant thickness, but a cascading vadose zone model allows it to resolve vertical variations in water content resulting from root water uptake, and the non-linear threshold-like spatial variations in the relationship between rainfall infiltration and groundwater recharge. The water table position responds to recharge from the vadose zone, and lateral flow calculated using Dupuit-like assumptions. A large subsurface thickness and permeability therefore endows a model landscape with not only the ability to rapidly drain saturated storage, but also the ability to absorb storm event rainfall in the vadose zone, especially when the evapotranspiration rate was also high relative to rainfall. The model showed that these characteristics resulted in less saturation excess overland flow compared to landscapes with poor subsurface drainage, as saturated areas were smaller and less responsive to storm events. Less surface runoff means less water-driven erosion, which means that at geomorphic steady state (when uplift balances erosion) diffusive hillslope erosion processes must be larger to compensate. The result is a landscape with higher relief and less drainage dissection (e.g., Perron et al., 2008).

While these model results indicate that the subsurface is a key link between topography and runoff generation, it is unclear whether these relationships can be observed in real landscapes. While field studies have shown that subsurface properties and topography have effects on hydrologic function (e.g., Prancevic & Kirchner, 2019; Jencso & McGlynn, 2011), relationships between subsurface properties and topography remain elusive (Luo et al., 2016; Sangireddy et al., 2016). Furthermore, it has proven challenging to show that such a relationship is the result of coevolution with hydrology (Yoshida & Troch, 2016). This lack of clear relationships is to be expected because hydrology, conditioned by climate, is only one connection between the subsurface and topography. Other controls include lithology and tectonic setting, which affect the styles and efficiencies of weathering, sediment particle size, and sediment transport; and vegetation, which alters subsurface properties and sediment transport efficiency through root growth, and hydrologic partitioning through evapotranspiration (Brantley et al., 2017; Collins & Bras, 2010).

In this paper we will look for evidence to support the hypothesis that subsurface thickness and permeability are important controls on surface topography (particularly relief and drainage density). We will apply the model of Litwin et al. (2024) to two locations where confounding differences are minimized, and there is a contrast in both the degree of topographic dissection and the subsurface properties. We aim to avoid calibration, relying instead in field observations, literature values, and topographic analysis to parameterize the model.

If the model is able to reproduce the distinct hydrologic and geomorphic properties of each site, this will lend strong credence to the arguments drawn from the model about how they are coupled, and the importance of subsurface properties in modulating that coupling. However, parameter uncertainty makes it very possible that the model will not reproduce the observed geomorphic length scales and hydrologic behaviour precisely. It is also possible that the process mechanisms we have chosen to encode in the model are not actually the processes most important at these sites (we will discuss this possibility later). If the model does not match the observations, or does so for the wrong reasons, it can still allow us to examine how sensitive model predictions are to subsurface properties given the realistic reference parameters the two sites provide. If the difference in model predictions between the sites align in magnitude and direction with observations from these sites this will provide (weaker, but defensible) support for the thesis.

1.2 Approach

We selected two sites where contrasting lithology results in a strong contrast in subsurface properties, but climatic and tectonic histories are similar because of their proximity. Our first site, Druids Run, is underlain by serpentine bedrock that forms thin rocky soil, while the second site, Baisman Run, is underlain by schist that weathers to form deep, permeable soil and saprolite. We will assume that the present hydrological function is adjusted to the watershed geomorphology, and that the terrain approximates a geomorphic steady-state, as suggested by (Pavich, 1989).

Given these differences in subsurface properties, insights gained from the analysis in Litwin et al. (2024) lead us to hypothesize that:

1. Saturated areas and storm runoff are larger and more variable in time at Druids Run than Baisman Run, and
2. Hillslopes are shorter and have less relief at Druids Run than Baisman Run.

Here we examine these hypotheses in three steps. First, we characterize the hydrological function and morphology of the two sites and evaluate whether they support these hypotheses. Second, we ask whether these differences could be accounted for by coevolution between runoff generation and erosion as conceptualised in our model. To do this we fully parameterize the landscape evolution model used in Litwin et al. (2024) without calibration and compare its predictions to the site properties. Third, we test whether subsurface hydrological differences are indeed the most important factors (or whether differences in other geomorphic properties can account for the different site morphologies) by performing a simple sensitivity analysis in which we swap the geomorphic process variables between the two sites while retaining the hydrologic and subsurface properties. The results reveal the relative importance of variations in subsurface hydrology relative to geomorphic process rates in explaining differences in emergent morphology and hydrologic function at these sites.

2 Materials and Methods

2.1 Site descriptions

Our study sites are located in the Piedmont physiographic province, north of Baltimore, Maryland. The climate is humid, with a mean annual precipitation of approximately 1150 mm and mean annual potential evapotranspiration of approximately 750 mm. There is no pronounced seasonality in precipitation, less than 5% of which falls as snow. Baisman Run is a 381 ha watershed in Oregon Ridge Park, defined by an outlet at (39.4795 N, 76.6779 W). Druids Run is a 107 ha watershed located in Soldiers Delight Natural Environment Area, and is defined by an outlet at (39.4171 N, 76.8523 W). The

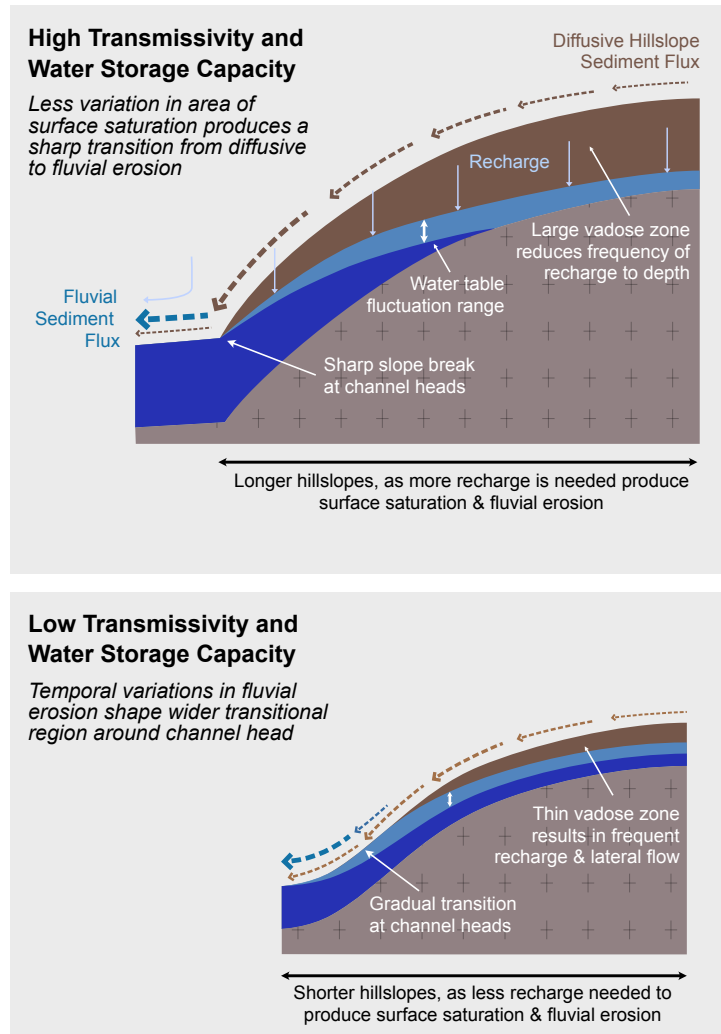


Figure 1. Conceptual figures showing a contrast in morphology and water table from ridge to channel head predicted by DupuitLEM. Gravity driven hillslope sediment flux moves material downslope proportional to the topographic gradient (brown dashed arrows). Water-driven fluvial erosion occurs where there is surface water, generated by precipitation on saturated areas and exfiltration (blue dashed arrows). When transmissivity and water storage capacity (drainable porosity integrated with depth) relative to storm event size are large, the subsurface can support long water flow paths before exfiltration, and the position where the water table intersects the surface is relatively static with time. When transmissivity and storage capacity are lower, hillslopes are shorter and the water table is more sensitive to time-varying recharge, such that the zone of surface water discharge and erosion varies in the vicinity of the channel head.

162 watersheds are 16 km apart, and are at approximately the same elevation (52 m and 56
 163 m above sea level respectively). Both watersheds drain to the Chesapeake Bay; Baisman
 164 Run drains via the Gunpowder River and Druids Run via the Patapsco River. Baisman
 165 Run has been monitored extensively as part of the Baltimore Ecosystem Study, and more
 166 recently as part of several projects aimed at improving understanding of deeply weath-
 167 ered critical zones (Putnam, 2018; Cosans, 2022). Druids Run has no prior description

or study. It is unnamed in the National Hydrography Dataset, so we unofficially named it in honor of a local group of druids that meet in the watershed.

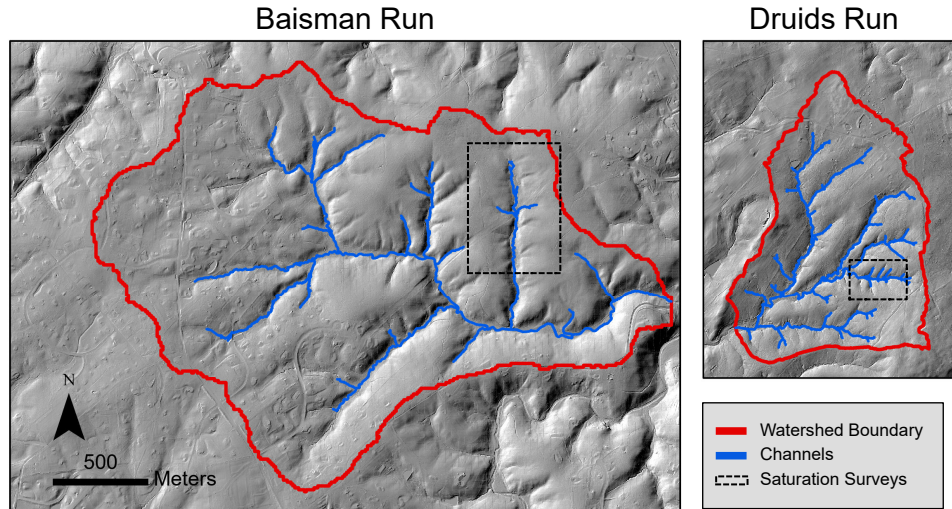


Figure 2. Hillshades of Baisman Run and Druids Run with the watershed boundary and channel network delineated with the DrEICH algorithm. Areas where we conducted saturation surveys (see Figure 5) are shown in dashed black boxes. The two sites are to scale, revealing the difference in their size and drainage dissection.

Baisman Run is underlain by the Loch Raven Schist (Crowley et al., 1975), a Cambrian-Devonian mica schist that has weathered to form deep, moderately permeable soil and saprolite. Drilling and geophysical measurements show that at the ridge, the depth to the saprolite-bedrock transition is ≈ 15 m and weathered bedrock extends several tens of meters further (Cosans, 2022). The depth to the saprolite-bedrock transition is much shallower in valley bottoms, $\approx 0-2$ m, as there are some bedrock outcrops appearing in channels (Cosans, 2022). The USDA maps the primary soils in the watershed as well-drained, loam to silt-loam textured with depth to water table and confining layer greater than 200 cm. Valley bottoms soils are poorly drained, with hydric-classified soils composing $\approx 3\%$ of the watershed (Staff & Natural Resources Conservation Service, United States Department of Agriculture., 2023). Agriculture was historically present in the eastern headwaters, where there is now suburban development, and a homestead and tree farm were historically present in the Pond Branch sub-watershed (Cleaves et al., 1970). The remainder of the watershed has been relatively undisturbed since the 1950s and today supports a mature deciduous forest.

Druids Run is primarily underlain by the Soldiers Delight Ultramafite (Guice et al., 2021). Soils are primarily classified as chrome silt loam, and are generally thin with a strong permeability contrast at the base of the A horizon (at an average depth of 46 cm). Ridgetop soil is rocky and can be as thin as 5 cm, and exposed bedrock is common near channel heads. In valley bottoms, alluvium and organic material accumulate to thicknesses around 1 m. Hydric-classified soils are found in some valley bottoms and compose $\approx 1\%$ of the watershed (Staff & Natural Resources Conservation Service, United States Department of Agriculture., 2023). The Soldiers Delight Ultramafite is host to a “serpentine barrens” ecosystem, which consists primarily of grasses and shrubs with some areas supporting hardwood and conifer trees. The Soldiers Delight area was mined for chromite in the 19th and 20th century. Several small pits are present near ridge crests

in Druids Run, and placer mining may have occurred in the valley bottoms, but the effects of this appear to be minimal in this watershed. Some structures and two small ponds are present in the upper portion of Druids Run, but most of the watershed is free from development.

2.2 Hydrological data

We combined existing hydrological data with new measurements of precipitation, streamflow, and saturated areas. Instantaneous precipitation rates were measured from June 2022 to February 2023 at a weather station located in an open field approximately 0.8 km north of Baisman Run. An identical unit was installed in an open area in Druids Run, which recorded instantaneous precipitation from April 2022 to February 2023. The stream gage at Baisman Run is operated and maintained by the U.S. Geological Survey (Gage 01583580). We established a new stream gage at Druids Run for this project.

The Druids Run stream gage is located at an existing concrete culvert crossing the stream channel. In April 2022 we installed a PVC housing on the concrete structure approximately 2 m from the culvert inlet. We measured water stage with a Solinst Leveller pressure transducer within that housing, and corrected for atmospheric pressure with a Solinst Barologger. The pressure transducer operated until the device failed in October 2022. Periodic discharge measurements were made to construct a rating curve. Low flows were measured with salt dilution gaging recorded with a HOBO conductivity logger, and high flows were measured using an OTT MF Pro electromagnetic current profiler. A power law model fit the stage-discharge data well, as shown in Figure S1.

While we do not have site-specific discharge uncertainty estimates, prior studies suggest reasonable and similar values. The U.S. Geological Survey reports gage discharge error is typically 3-6%, and rarely up to 20% (Sauer & Meyer, 1992). Schmadel et al. (2010) conducted an in-depth uncertainty analysis of discharge estimated from a dilution gaging procedure very similar to ours and found approximately 8% error.

We surveyed limited areas of both watersheds manually for saturation conditions between April 2022 and March 2023. At Baisman Run, the surveys were conducted in the headwaters of the Pond Branch sub-watershed. At Druids Run, they were conducted in a headwater catchment near the eastern watershed boundary. We measured saturation at points along predefined transects, and returned to the approximate (but not exact) positions for each survey. We selected transects to balance capturing a range of hillslopes, zero- and first-order channels, while covering a small enough area to avoiding significant changes in saturation over the course of a measurement campaign. Saturation was measured by walking the transects, and pushing a rebar rod approximately 2 cm into the ground and moving the rod up and down in the shallow hole. Points along these transects were recorded as not saturated if no squishing sound was heard (N), soil-saturated if a squishing sound was heard (Ys), ponded (Yp), or flowing (Yf) if water was observed on the surface. Three close locations were measured at each point on the transect, and the highest category in this hierarchy was recorded as the value (e.g., if two points did not squish, but one did, the recorded class would still be Ys). This procedure was repeated under different discharge and moisture conditions.

2.3 Hydrological analysis

Valuable information about contributing areas can be extracted from rainfall and runoff timeseries. The event runoff ratio, defined as the ratio of the total event runoff to event precipitation, can approximate the proportion of the watershed contributing storm runoff (e.g., O'Loughlin, 1986). To calculate event runoff, we first separated the discharge timeseries into baseflow and quickflow using the graphical approach described by Hewlett

and Hibbert (1967). Because hydrograph separation only delineates by timescale of response (fast versus slow), the resulting event runoff does not necessarily derive from a particular runoff pathway, such as runoff from saturated areas. Still, the event runoff ratio can provide an indication of the relative watershed connectivity that drives rapid runoff response to rainfall.

Using the method of Hewlett and Hibbert (1967), baseflow is equal to discharge and quickflow is zero until discharge increases at a rate faster than $0.000546 \text{ m}^3 \text{ s}^{-1} \text{ km}^{-2} \text{ h}^{-1}$. Baseflow continues to increase at this rate until discharge declines and is equal to baseflow. Storm events are periods where quickflow is greater than zero and the rise is associated with precipitation. Corresponding precipitation events start t_0 hours before event quickflow begins, and end t_1 hours before discharge returns to baseflow, where t_0 and t_1 are fixed values for each site. By examining precipitation and discharge timeseries, we found that $t_0 = 2$ hours and $t_1 = 1$ hour were appropriate for Druids Run, and $t_0 = 6$ hours and $t_1 = 2$ hours were appropriate for Baisman Run. We excluded runoff events shorter than 6 hours because these generally had small discharge responses relative to noise in the timeseries.

While the runoff ratio provides a signature of contributing area, the saturation dataset provides a direct means to assess the variability of saturated areas. The saturation surveys yielded categorical data that vary with topographic position and catchment discharge. To develop quantitative insights from the dataset, we first created a binary classification of whether points were not saturated (N) or saturated (Ys, Yp, Yf). We then used logistic regression to generalize our discrete measurements to predictions of how saturation probability p varies in space, assuming similarity with topographic (wetness) index $TI = \frac{A}{v_0|\nabla z|}$ (Beven & Kirkby, 1979), and in time assuming similarity with baseflow discharge Q_b :

$$\log\left(\frac{p}{1-p}\right) = \alpha_0 + \alpha_1 \log\left(\frac{A}{v_0|\nabla z|}\right) + \alpha_2 \log\left(\frac{Q_b}{A_{tot}}\right) \quad (1)$$

where $A(x, y)$ is the area upslope of a contour width v_0 , $|\nabla z(x, y)|$ is the topographic slope, and A_{tot} is the total watershed area. The model parameters are α_0 , α_1 , and α_2 .

To calculate topographic index, we first resampled the DEM to 5 m resolution to smooth over roughness in the high resolution DEM and to reflect the uncertainty in the positioning data of our saturation surveys. The resampling approach is also consistent with our measurement scheme, in which we labeled locations based upon the highest saturation class observed in a small vicinity. We calculated upslope area using the D_∞ algorithm, and slope using the same 10 m footprint used to calculate hilltop curvature. While our regression model calls for the use of baseflow discharge, we used the total discharge, as all of our samples were taken during baseflow or recession periods. This was also necessary because the timeseries of discharge at Druids Run did not overlap all the saturation surveys. For consistency, we used instantaneous discharge measurements from immediately before the surveys began. At Druids Run, we made these measurements using dilution gaging; at Baisman Run, we used instantaneous discharge from the USGS gage.

2.4 Hillslope length and relief

We conducted geomorphic analyses using a lidar-derived digital elevation model with 0.76 m resolution, which was collected in 2015 and is publicly available from Baltimore County. We conducted all topographic analyses using LSDTopoTools (S. Mudd et al., 2022). To determine hillslope length and relief, we began by identifying the channel networks at both sites using the DrEICH algorithm (Clubb et al., 2014). DrEICH uses χ -analysis (Perron & Royden, 2013) to locate channel heads at the transition point from linear channel segments to nonlinear hillslope segments in χ -elevation space. χ -analysis is discussed in more detail in Section 2.7.2. We adjusted the DrEICH model parameters

such that the predicted channel network matched observed channel network in the sub-watersheds where we measured saturation. The channel network in these areas was observed visually in the field as the extent of fluvial incision with clear connection to larger channel baselevel. We then used the channel network to identify hilltops, which are defined as edges shared by watersheds with the same Strahler stream order (Hurst et al., 2012). Finally, we calculated hillslope length as the steepest descent distance from each hilltop point to the nearest channel point, and hillslope relief as the hilltop elevation above the nearest channel point (Grieve et al., 2016).

2.5 Landscape evolution model

We use the landscape evolution model described by Litwin et al. (2024) to understand the sensitivity of topography and runoff generation to subsurface properties and geomorphic process rates for cases similar to those we observe at these sites. As this is a reduced complexity model intended for long-term evolution, and is initialized with small random elevation perturbations, we do not expect the model to reproduce the arrangement of streams and ridges at our sites. Rather we will measure key metrics of the landscape, including hillslope length and local relief, and compare these to the site.

The model accounts for topographic evolution due to baselevel change, water-driven erosion using the streampower erosion equation, and hillslope sediment transport using a nonlinear hillslope diffusion equation. We decided to use a linear diffusion formulation, as the hillslopes at Baisman Run and Druids Run generally remain convex until they reach valley bottoms, and the topography shows no evidence of shallow landsliding or other mass movements. The subsurface maintains constant and spatially uniform properties through evolution, implicitly assuming that the production of permeable material keeps pace with surface erosion. The overland flow that drives fluvial erosion is generated by exfiltration and precipitation on saturated areas where the shallow aquifer reaches the land surface. The shallow aquifer model uses the Dupuit-Forcheimer assumptions to calculate flow over a sloping impermeable base. The aquifer receives recharge from the vadose zone, which is represented using a single 1-dimensional profile in which discrete depth increments fill and drain by the plant-available water capacity in the increment. The profile dynamics are described by Schenk (2008). Evapotranspiration draws water from the shallowest available depth increment, and infiltration displaces water from the surface further into the profile. From this single profile, recharge is calculated at each aquifer node by mapping the amount of water that infiltrates into the profile below the water table depth. This one-directional coupling is computationally efficient but means that the saturated zone cannot affect vadose water storage (such as through capillary rise) or supply water for evapotranspiration. The climate is treated as a simple (Poissonian) random jump process, following Eagleson (1978), with exponentially distributed storm depth, duration, and interstorm interval, and constant evapotranspiration at the climatological mean rate during the interstorm periods.

We ran the model under the same initial and boundary conditions used in Litwin et al. (2024). The domain is square. One side boundary is fixed to baselevel, while the remaining three side boundaries are zero-flux. We began with a flat initial surface at baselevel, add small random perturbations, and simulate 50 Ma of evolution until a dynamic equilibrium between erosion and uplift is reached. While this timescale is long relative to periodic changes in climate and baselevel in the Eastern Piedmont (e.g., Cleaves, 1989), we know that both sites have experienced the same forcings through their evolution, such that a single climate and baselevel change rate should still provide insights into their evolution.

2.6 Hydrological parameters

2.6.1 Transmissivity, hydraulic conductivity, and permeable thickness

The maximum transmissivity (hereafter just *transmissivity*) is defined as the depth-integrated saturated hydraulic conductivity. It appears in our model as the product of the effective saturated hydraulic conductivity k_s and permeable thickness b . We developed a novel method to use the saturation survey data to estimate a catchment-averaged transmissivity, building on an existing approach. We then divided that value into estimates of k_s and b .

Our method of estimating transmissivity is similar to that described by O’Loughlin (1986), as it is built on a steady state hillslope water balance and the assumption that places with the same topographic wetness index TI saturate at the same time (Beven & Kirkby, 1979). The approach begins by considering recharge that is supplied at a rate $r(x, y)$ to the saturated zone. At hydrologic steady state, the total water outflow along a topographic contour segment with length v_0 is equal to the integral of recharge over the area upslope of the contour A_c . In this way, convergent slopes will saturate before planar and divergent ones. The maximum amount of recharge that can be moved through the subsurface before saturation occurs depends on the transmissivity T and the local hydraulic gradient, which is assumed to be equal to the topographic gradient ∇z . As a result, the criterion for saturation at the contour segment is:

$$\int_{A_c} r(x, y) dA \geq T |\nabla z| v_0. \quad (2)$$

At saturation, any additional recharge will become overland flow. Because in general the recharge is not known, O’Loughlin (1986) equated the total watershed recharge with the watershed baseflow Q_b :

$$\int_{A_{tot}} r(x, y) dA = Q_b, \quad (3)$$

where A_{tot} is the watershed area. From this expression, we derived an average recharge rate $\bar{r} = Q_b/A_{tot}$. Dividing Equation 2 by the average recharge rate equation and rearranging the terms, we derived an expression for the discharge-normalized transmissivity:

$$\frac{1}{|\nabla z| v_0} \int_{A_c} \left(\frac{r}{\bar{r}} \right) dA \geq \frac{T}{Q_b/A_{tot}}. \quad (4)$$

By further assuming that the integrand in the above expression is approximately unity, we obtain an expression that relates the topographic index to transmissivity and base-flow discharge:

$$\frac{A}{|\nabla z| v_0} \geq \frac{T}{Q_b/A_{tot}}. \quad (5)$$

where A/v_0 is the upslope area per contour width, calculated at every point in the landscape using the digital elevation model. We will call the topographic index at boundary between saturated and unsaturated ground TI^* , which is a function of discharge Q_b . At that value the inequality in the expression above becomes equality. Using a log transform, we derived an expression for the log of transmissivity:

$$\log(T) = \log(TI^*) + \log\left(\frac{Q_b}{A_{tot}}\right). \quad (6)$$

To find T using this expression and our saturation surveys, consider a logistic regression model with the form:

$$\rho(p) = \log\left(\frac{p}{1-p}\right) = \beta_0 + \beta_1 \log\left(\frac{A}{v_0 |\nabla z|} \frac{Q_b}{A_{tot}}\right) \quad (7)$$

where β_0 and β_1 are parameters of the regression model. This logistic regression model is very similar to that in Equation 1, but has one fewer parameter, and consequently enforces that the odds of saturation are log-linearly dependent on the product of Q_b and

TI . At the critical value of topographic index TI^* , we will call the odds of saturation ρ^* :

$$\rho^* = \beta_0 + \beta_1 \log \left(TI^* \frac{Q_b}{A_{tot}} \right). \quad (8)$$

Finally, we rearranged Equation 8 to match the form of Equation 6, and solved for the transmissivity:

$$T = e^{(\rho^* - \beta_0)/\beta_1}. \quad (9)$$

The main difference between this approach and that described by O’Loughlin (1986) is that their approach equates the ratio of quickflow to precipitation with the proportion of the watershed that is saturated, while we have direct estimates of how saturation varies with baseflow and topographic index. This should make our approach more robust, though it is still limited to the steady-state hydrological theory from which it was derived. Finally, we partitioned transmissivity between permeable thickness b and an effective saturated hydraulic conductivity k_s based on permeable thickness values taken from the USDA Soil Survey (Staff & Natural Resources Conservation Service, United States Department of Agriculture., 2023) and insights gained from prior subsurface investigations of Baisman Run.

2.6.2 Drainable porosity and plant available water content

Drainable porosity n_e relates the depth of water stored or released when there is a change in water table elevation. Estimates usually require either hydraulic well tests or laboratory analyses. In the absence of hydraulic test data or permission to take soil samples from Druids Run, we assumed that the drainable porosity was the same at both sites. Plant available water content (n_a) is the amount of water available for plant use per unit volume of soil. The values were estimated based on the USDA Soil Survey data for the dominant soil types at the two sites.

2.6.3 Climatological parameters

We fit three independent exponential distributions for storm depth d_s , duration t_r , and interstorm duration t_b by calculating the mean values of these quantities from a precipitation dataset previously collected from 2014-2018 at the weather station at Baisman Run (Cosans, 2022). Because the two sites are very close together, this one time-series was used to calculate storm statistics at both sites. The distributions are:

$$f(d_s) = \frac{1}{\langle d_s \rangle} \exp \left(- \frac{d_s}{\langle d_s \rangle} \right) \quad (10)$$

$$f(t_r) = \frac{1}{\langle t_r \rangle} \exp \left(- \frac{t_r}{\langle t_r \rangle} \right) \quad (11)$$

$$f(t_b) = \frac{1}{\langle t_b \rangle} \exp \left(- \frac{t_b}{\langle t_b \rangle} \right) \quad (12)$$

$$(13)$$

where the angled braces indicate the temporal mean of the quantity. Potential evapotranspiration (ET) was estimated based on the average annual value in Baltimore between 1981 and 2010, as reported by the Northeast Regional Climate Center at Cornell University. In our model, ET only occurs during interstorm periods, so the interstorm potential ET rate pet was estimated by rescaling the average potential ET rate with the interstorm time fraction. Our climatological approach is simplistic, neglecting covariance of storm depth, duration, and interstorm duration, seasonality, paleoclimatic variability, and so on. However, we do not expect any large differences in the climate between the two sites, so even a simple approach should allow us to make comparisons of how landscapes with different geomorphic and subsurface hydrologic properties respond to climatic conditions similar to those observed at our sites.

2.7 Estimating geomorphic parameters

The topographic parameters of our model are the uplift or baselevel change rate U , hillslope diffusivity D , streampower incision coefficient K , characteristic contour width v_0 , and the streampower exponents m and n , as discussed below. The Piedmont is thought to reasonably approximate geomorphic steady state (Pavich, 1989; Bazilevskaya et al., 2013), so we set the rate of baselevel fall equal to the average cosmogenic ^{10}Be erosion rate from nearby Piedmont sites. The remaining parameters were identified using topographic analysis. The methods presented below are largely consistent with methods used by others in the literature, except for the streampower parameters. There we present a modification of a previously-proposed method, adapted to account for the effect of hydrologic variability.

2.7.1 Hillslope diffusivity

Hillslope diffusivity can be derived from the rate of baselevel change U and hilltop curvature C_{HT} (Roering et al., 2007; Hurst et al., 2012):

$$D = -\frac{U}{C_{HT}}. \quad (14)$$

In hillslope evolution contexts, it is typical to account for the ratio of the bulk densities of regolith (on which the diffusion process occurs) and parent material (on which baselevel change occurs) (Roering et al., 2007). Because we are working with an integrated channel and hillslope model, and we do not have good estimates for the bulk density of fluvially-eroded material, we will neglect the bulk density terms. In this context, D is an effective diffusivity that will match the simulated hilltop curvature with that from our topographic measurements. We calculated the hilltop curvature by taking the second derivative of a polynomial surface fit to a 10 m footprint around each hilltop point. Hilltop points are the same as those used for the hillslope length analysis. The footprint size was selected by calculating the hilltop curvature for footprints of varying sizes and selecting the size at which there is a break in the standard deviation of curvature, following the procedure described by Hurst et al. (2012).

2.7.2 Streampower parameters

We estimated the streampower law parameters using an integral approach called χ -analysis (Perron & Royden, 2013). While the parameters can be derived from slope-area analysis, slope estimates often have significant noise that can result in poor parameter estimates (Perron & Royden, 2013). The integral approach is more stable, as it only requires the elevation and the upslope area to calculate the model parameters. The typical χ -analysis needed slight modification to accommodate our landscape evolution model. Litwin et al. (2022) derived the fluvial incision term of the landscape evolution model with assumptions that yielded linear dependence on the dimensionless discharge Q^* , a slope exponent $n = 1$, and area exponent $m = 1/2$. We derived a more general form by assuming that the exponent that determines the channel width from area and the exponent that determines erosion rate from shear stress were free parameters:

$$E_f = KQ^{*n} (v_0 a)^m |\nabla z|^n \quad (15)$$

where E_f is the fluvial incision rate, K is the erodibility, v_0 is the characteristic contour width, a is the area per contour width, and ∇z is the elevation gradient. For simplicity, we will use the variable Q^* to refer to the temporally-averaged dimensionless discharge which is called $\langle Q^* \rangle$ in Litwin et al. (2024). Because χ -analysis is usually only applied to river channels, it is typical to neglect the hillslope diffusion term, and write the solution at equilibrium between uplift and fluvial incision along a channel distance coordinate x :

$$U = KQ^{*n} (v_0 a)^m \left| \frac{\partial z}{\partial x} \right|^n. \quad (16)$$

We then solved for $|\partial z/\partial x|$, and substituted area for area per contour width times the characteristic contour width $A = v_0 a$:

$$\left| \frac{\partial z}{\partial x} \right| = \left(\frac{U}{K Q^{*n}} \right)^{1/n} A^{-m/n}. \quad (17)$$

Next we normalized upslope area to a reference drainage area A_0 , and integrated the equation above with respect to x :

$$z(x) = z(x_b) + \int_{x_b}^x \left(\frac{U}{K Q^{*n} A_0^m} \right)^{1/n} \left(\frac{A_0}{A(x)} \right)^{m/n} dx \quad (18)$$

where $z(x_b)$ is the elevation at a specified baselevel location x_b . In general, Q^* varies with position, so we cannot remove it from the integral. However, in our model Q^* generally approaches a constant value as you move downstream equal to one minus the actual evapotranspiration relative to precipitation $1 - \langle AET \rangle / \langle P \rangle$, which is approximately the mean runoff ratio $\langle Q \rangle / \langle P \rangle$. We will call this value Q_{max}^* . Then we can write:

$$z(x) = z(x_b) + \left(\frac{U}{K Q_{max}^{*n} A_0^m} \right)^{1/n} \chi, \quad (19)$$

where

$$\chi = \int_{x_b}^x \left(\frac{A(x)}{A_0} \right)^{m/n} dx. \quad (20)$$

These equations show that the elevation of a stream channel in dynamic equilibrium should be linear with respect to χ if U , K , and Q_{max}^* are uniform, and that the slope of that relationship should be:

$$k_{sn} = \left(\frac{U}{K Q_{max}^{*n} A_0^m} \right)^{1/n}, \quad (21)$$

which is often called the normalized channel steepness index. Note that this is related to but distinct from our use of “steepness” in Litwin et al. (2022).

We calculated the slopes of channel segments in χ -elevation space for the channel networks we extracted previously. Because the reference drainage area A_0 is introduced for dimensional purposes only, we can set it equal to unity, and solve for the streampower incision coefficient K :

$$K = \frac{U}{(k_{sn} Q_{max}^*)^n}. \quad (22)$$

3 Results

3.1 Hydrologic and geomorphic observations

3.1.1 Discharge, baseflow, and runoff ratio

Figure 3 shows the timeseries of discharge and precipitation for both sites. Baseflow (in dark blue) at Baisman Run declined from early summer continuing until October, when a small persistent increase is combined with episodic increases in response to large storms. Unfortunately the discharge timeseries available to us at Druids Run is too short to look at annual trends, though there does appear to be a significant baseflow decline from spring into summer, leading to low flows by late June. We did not observe no-flow conditions at the gage location, but we do know that flows were often close to or below the pressure transducer detection limit during the summer.

The storm runoff ratio is substantially more variable at Druids Run than Baisman Run. We identified 21 storm events at Druids Run and 43 storm events at Baisman Run, and found that the total event precipitation explained most of the variation in total event quickflow $Q_{f,event}$ (Figure 4). Events are colored by the antecedent baseflow, which shows

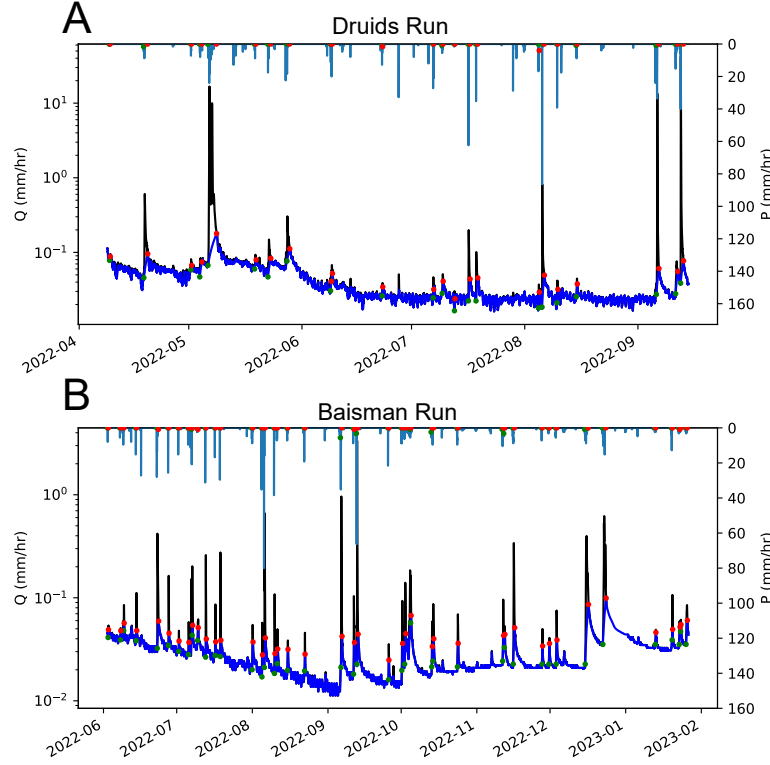


Figure 3. Timeseries of discharge Q (black), baseflow Q_b (dark blue), and precipitation P (light blue) at Druids Run (A) and Baisman Run (B). Storm events that we identified based upon the baseflow separation and precipitation begin with green dots and end with red dots, which are placed at the corresponding times on both the precipitation and discharge timeseries. Note that the timeseries for Baisman Run and Druids Run are not aligned in time.

that some of the variation in event runoff that cannot be explained by event precipitation may be explained by antecedent conditions. To quantify the sensitivity of event runoff to event precipitation, we fit the curve $Q_{f,event} = a_2 P_{event}^{a_1}$, where the log-space slope corresponds to the fitted exponent a_1 . The exponent and standard error are 3.17 ± 0.40 and 1.89 ± 0.13 at Druid Run and Baisman Run, respectively. An exponent $a_1 = 1$ would indicate that the storm runoff is a constant proportion of the event precipitation. When the event runoff ratio is interpreted as the effective proportion of the watershed contributing runoff (O'Loughlin, 1986), an exponent closer to one indicates that the contributing area does not vary with storm size. This interpretation suggests that contributing areas vary with precipitation at both sites, but they are more variable at Druids Run than Baisman Run. This interpretation also suggests that as storm events approach 100 mm, nearly all of Druids Run contributes storm runoff (4A). These events are fairly frequent; the annual maximum recurrence interval of 100 mm of precipitation in 24 hours is approximately two years at our sites (NOAA, 2024).

3.1.2 Saturated areas

At Druids Run, observed saturation was highly variable in time and correlated with discharge. We measured saturation five times along nine transects, seven of which run along first order drainages or the interfluvies between them, and two of which run par-

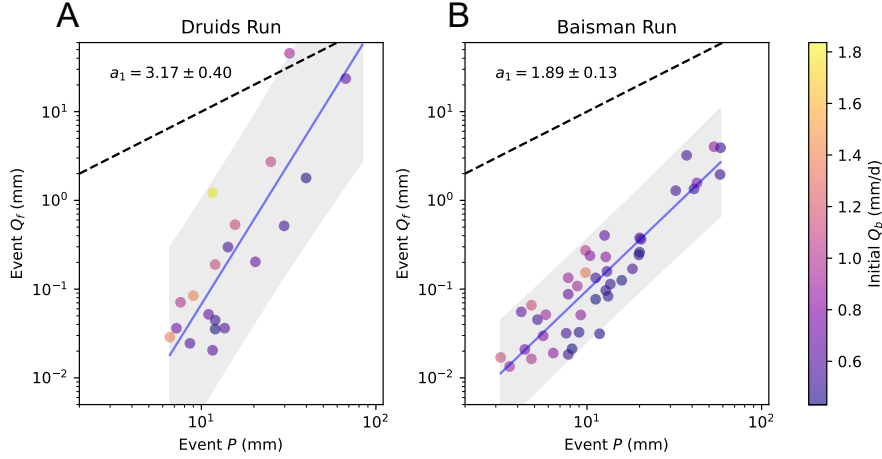


Figure 4. Event runoff characteristics for Druids Run (A) and Baisman Run (B). Event totals are calculated by summing the 15-minute precipitation and quickflow timeseries over the event durations. The points are colored by the initial baseflow Q_b . The dotted line is a 1:1 line, which represents the case where event runoff is equal to event precipitation. The blue line is a power law regression with the form $Q_{f,event} = a_2 P_{event}^{a_1}$, and the shaded area is the 95% confidence interval on the regression. The range on the coefficient a_1 is given as the standard error.

allel to the valley bottom (Figure 5A–E). The surveys conducted under the two highest flow conditions (C, E) had the greatest number of saturated points. Saturation was often discontinuous with distance downstream in first order channels. Upslope areas sometimes saturated and flowed first, while downslope reaches remained dry, as flow passed through the subsurface. First order channels tend to have exposed bedrock or thin alluvial cover near their headwaters, while closer to the valley bottom they become submerged in alluvium that has sufficient capacity to move the water from upslope through the subsurface. Bedrock fractures may also play a role in redistributing surface flow to subsurface pathways.

In contrast, saturated areas were more persistent at Baisman Run. We measured saturation four times along six transects, four of which run perpendicular to the valley bottom, and two run parallel to it (Figure 5F–I). Regardless of discharge, we found that saturation was confined to locations at or below the distinct break in slope where the hillslopes meet the valley bottom. Within the valley bottom, saturation was not present everywhere, as the stream channel is incised into the valley bottom alluvium in some places. Flow emerges at distinct springs and seeps at the break in slope (Putnam, 2018). The springs are further evidence that subsurface pathways support baseflow, while the relatively persistent nature of saturated areas support our observation that event quickflow is less sensitive to event precipitation at Baisman Run than it is at Druids Run.

We used the logistic model (Equation 1) to predict the odds of saturation for the range of topographic index values in each watershed and the range of discharge values at which saturation surveys were conducted (Figure 6). The parameters of the fitted model are shown in Table 1. In Figure 6, the topographic index value at which the black dashed line intersects the odds ratio curves is the critical value of TI where saturation becomes more likely than not for a given value of discharge. We plotted this together with the probability density of watershed topographic index (orange) to show how the critical TI relates to the distribution of TI for the watershed.

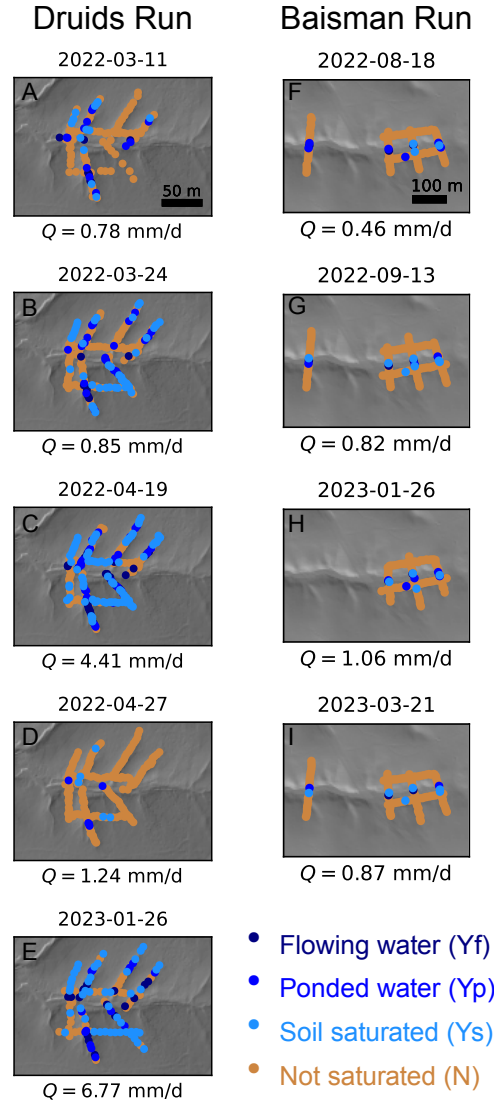


Figure 5. Observations of saturation made on transects at Druids Run (A–E) and Baisman Run (F–I). The latter plots have been rotated 90 degrees such that north is in the direction of the positive x-axis. In both figures, flow in the valley bottom is from right to left. The classification and sampling approaches are described in Section 2.2.

	α_0	α_1	α_2
Druids Run	4.609 ± 0.637	0.174 ± 0.040	1.000 ± 0.097
Baisman Run	-7.559 ± 4.299	0.703 ± 0.103	0.070 ± 0.590

Table 1. Estimated parameter values of the logistic regression models for saturation (Equation 1), where α_0 is the intercept, α_1 is the coefficient on topographic index, and α_2 is the coefficient on the area-normalized discharge. Parameter ranges are given as standard errors.

The regression model for Druids Run in Figure 6A shows that the predicted odds of saturation varies substantially with discharge. When discharge is small, the critical TI value confines likely saturation to a very small portion of the total watershed area, while for large discharge the critical value of TI is low enough that most of the watershed is likely to be saturated. This supports the high variability of saturation in space and time that we inferred from the pointwise measurements.

The logistic regression model predicts very different behavior for Baisman Run (Figure 6B). First, we notice that the saturation odds curve does not vary with discharge, such that all curves overlap. This is reflected in the regression parameter α_2 on discharge (Table 1), which is much smaller and more uncertain for Baisman Run than Druids Run. As a result, the critical value of topographic index is nearly constant with time. Second, we notice that the curves are narrower and steeper than those estimated for Druids Run, such that the odds of saturation increases more abruptly around the critical value of TI . This is reflected in the regression parameter α_1 on topographic index, which is much larger at Baisman Run than Druids Run. This supports our observation that saturation emerges abruptly at the transition from hillslopes to valley bottoms.

The logistic regression models also allowed us to generalize the saturation predictions to the entire watersheds. We predicted saturation through time for the discharge timeseries in Figure 3 and for all raster points based upon their topographic index. We then classified whether each point was “wet” (exceeded criteria for saturation greater than 95% of the time), “dry” (exceeded criteria for saturation less than 5% of the time), or variably saturated if it met neither of those criteria.

Figure 7 shows a dramatic difference in the hydrological function of the two sites based on the logistic regression model predictions. The predicted channel network at Druids Run was ephemeral until close to the watershed outlet. Variable saturation is widespread in zero-order basins and onto some hilltops, but as Figure 6A shows, saturation at these locations with low topographic index only occurs at the high discharge values, which are associated with storm events. Some of the hillslopes we sampled that appear as “dry” may in fact saturate occasionally, but less than 5% of the time. In contrast, the regression model predicted that Baisman Run had a continually wet stream channel over the course of our observation period, and did not experience saturation on the hillslopes.

Analysis of rainfall-runoff and saturation data reveal the dramatic difference between hydrological function of the two sites. When the permeable subsurface is thin, as at Druids Run, much of the landscape saturates and desaturates relatively easily in response to precipitation, and the effective proportion of the watershed contributing runoff varies substantially. In contrast, when the permeable subsurface is thick, as at Baisman Run, the same precipitation causes modest or no change in saturated areas, though new subsurface flow paths may still be activated with increasing storm size, such that the effective contributing area increases with increasing wetness.

The dynamics of saturated areas with discharge can be considered an extension of work on flowing channel length dynamics (e.g., Prancevic & Kirchner, 2019). Our results

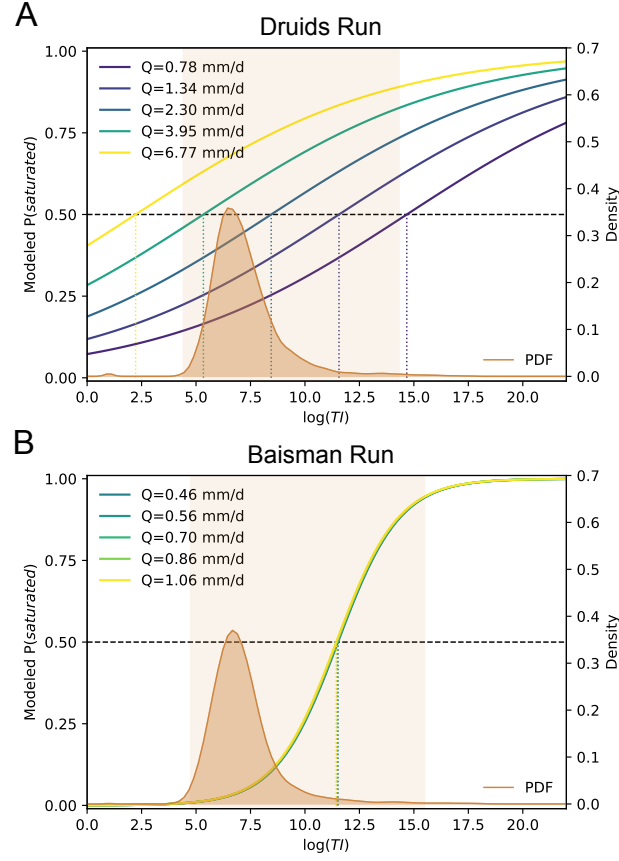


Figure 6. Regression results for Druids Run (A) and Baisman Run (B). The regression model has the form given in Equation 1. The modeled probability of saturation is given in terms of topographic index and discharge, where discharge varies logarithmically across the range of saturation survey discharge values. There is a dashed line at the 50% probability mark, and where this intersects each one of the probability curves, there is a dotted line dropped to the x-axis. This indicates the critical value of topographic index at which saturation is more likely than not to occur given that value of discharge. On the opposing axis is the probability density of topographic index, estimated with a kernel density approach. The lighter shaded region indicates the range of TI values sampled in our surveys, which indicates good topographic index coverage of our samples.

also show that the dynamics of saturation depend on a balance of upslope water supply and downslope transport capacity, which can be related to subsurface properties and topography.

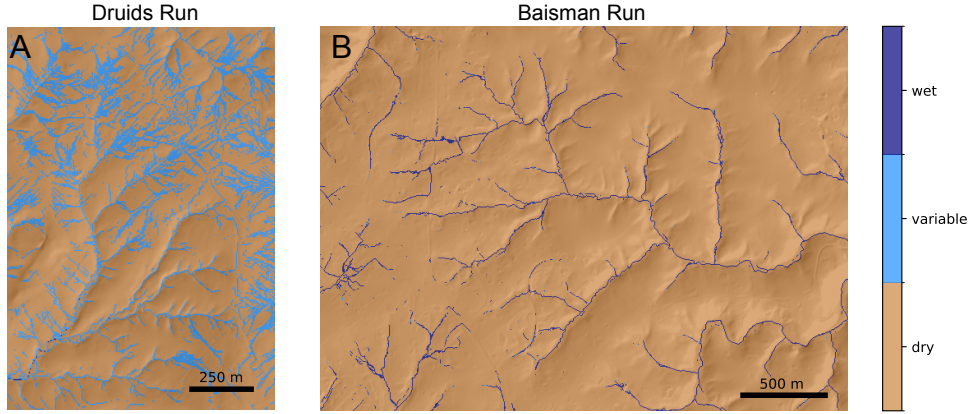


Figure 7. Classified saturated areas for Druids Run (A) and Baisman Run (B), based on the logistic regression model in Equation 1 and shown in Figure 6, and the runoff timeseries shown in Figure 3. The modeled probability necessary for saturation was set at 50%. A location was classified as “wet” if it exceeded criteria for saturation greater than 95% of the time, “dry” if it exceeded criteria for saturation less than 5% of the time, or variably saturated if it was in between.

3.1.3 Hillslope length and relief

Both hillslope length and relief are greater at Baisman Run than Druids Run. The channel networks and hilltop points from which hillslope length and relief were defined are shown in Figure 2. Totals of 5.3×10^4 and 7.0×10^4 hilltop points with unique length and relief were identified at Druids Run and Baisman Run, respectively. The median hillslope length is 88.3 m at Druids Run and 177.3 m at Baisman Run, while median relief was 2.9 m at Druids Run and 6.7 m at Baisman Run. In trying several other channel network extraction methods, we found that the hillslope length distributions varied but that hillslopes were still generally shorter at Druids Run than Baisman Run. Figure 8A shows that there is no overlap in the interquartile range (IQR) of hillslope length or relief for the two sites. The strength and sign of this difference supports our hypothesis that the site with a thick permeable subsurface will have greater hillslope length and relief than that with a thin permeable subsurface.

3.2 Landscape evolution parameterization

While both the hydrological and geomorphic differences between Druids Run and Baisman Run support our hypotheses, we have not yet established that the subsurface is the link between the emergent hydrological function and morphology. To do so, we estimated the parameters for DupuitLEM, and ran the model under conditions that approximate those found at our sites. Using the approaches described in Sections 2.6 and 2.7, we estimated all the parameters needed to run the model without calibration. Parameters are estimated independently from one another, though we assume that both sites have experienced the same uplift rate U .

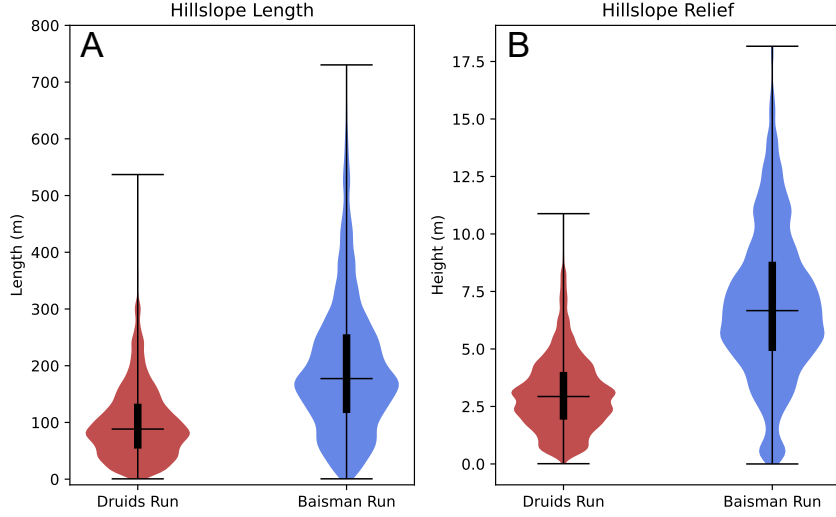


Figure 8. Violin plots of hillslope length and relief for Druids Run (A) and Baisman Run (B). Hillslope length is the length along a flow path from a hilltop point to the nearest channel point along a flowpath. Hillslope relief is the drop in elevation over that distance. Violin plots show the median, minimum, and maximum (horizontal lines) values and the interquartile range (wider vertical bar).

3.2.1 Hydrologic parameters

We first estimated the transmissivity using Equation 9. We estimated the parameters β_0 and β_1 by fitting Equation 7 using topographic index, discharge, and saturation survey data. With the fitted model, we determined the optimal threshold probability p^* at which saturation was likely to occur. While we could have chosen 50% as we did in the regression model for saturated area, we found that this performed poorly on the simpler two-parameter formulation used to calculate transmissivity. The selected value of p^* should balance correctly classifying points as saturated (high true positive ratio (TPR)) and minimizing the number of points that are misclassified as saturated (low false positive ratio (FPR)). Plotting TPR against FPR gives the receiver operating characteristic curve, from which we selected the optimal threshold probability by maximizing the difference TPR-FPR. The results of this process are shown in Figure 9. Using the optimal p^* , we estimated the transmissivity from Equation 9 10,000 times using Monte Carlo simulations to determine the uncertainty due to the variance and covariance of the logistic regression parameters. The median and quartiles of transmissivity are reported in Table 2. This approach predicts that the transmissivity at Baisman Run is nearly 3.5 times higher than at Druids Run. There is no overlap between the IQRs of the estimated transmissivities, which suggests a robust difference between the two sites. The uncertainty we have quantified reflects that of the regression parameters, but does not include the optimal threshold predicted by maximizing TPR-FPR. The ambiguity in the peak value (Figure 9D) suggests that transmissivity and its uncertainty may be larger than we have predicted. There is also uncertainty related to methodological choices (raster resolution, flow routing method, threshold selection method), but experimentation suggested that the median transmissivity is always larger at Baisman Run than Druids Run when the same methodology is applied to both sites.

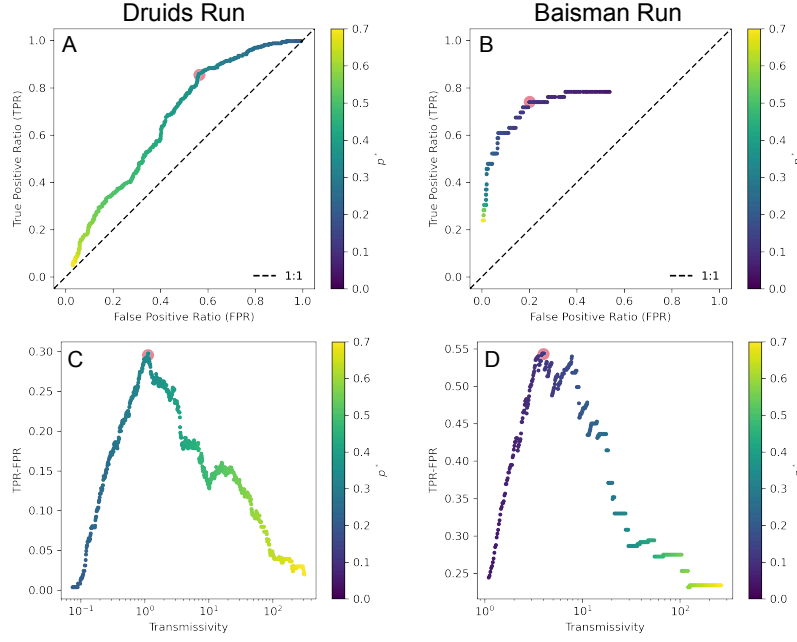


Figure 9. Results of the TPR-FPR analysis. (A–B) The receiver operating characteristic curve for Druids Run and Baisman Run, respectively, colored by the threshold value p^* used to obtain each combination of quantities. (C–D) The difference TPR-FPR, which we seek to maximize, plotted against the transmissivity value associated with each threshold p^* . We selected the transmissivity associated with the largest value of TPR-FPR.

	Transmissivity (m^2/d)			Regression Parameters			
	Med	LQ	UQ	$\bar{\beta}_0$	$\bar{\beta}_1$	ρ^*	p^*
Druids Run	1.12	0.88	1.40	-0.691	0.268	-0.660	0.341
Baisman Run	3.89	3.24	4.64	-3.012	0.693	-2.072	0.112

Table 2. Median (Med), lower and upper quartiles (LQ, UQ) of transmissivity estimated from the logistic regression model, and the associated regression model parameters. The bar over a variable indicates the mean value.

To estimate the effective hydraulic conductivity from transmissivity, we first estimated the permeable thickness. At Druids Run, data from the USDA Soil Survey suggested a strong permeability contrast at the base of the A horizon, so we used the characteristic A horizon thickness as our permeable thickness (Staff & Natural Resources Conservation Service, United States Department of Agriculture., 2023). At Baisman Run, there is no strong permeability contrast within the soil profile, so we used the entire soil profile thickness, weighted for the different soil types found in the watershed (2.03 m). We added 2 m to this value to approximate the average saprolite thickness between ridges and valleys in Baisman Run (Cosans, 2022). Our model is generally less sensitive to thickness than to maximum transmissivity, so we do not expect the results to be highly sensitive to the possible range of this value (Litwin et al., 2022, 2024). We divided transmissivity by the permeable thickness, and found that the effective hydraulic conductivity is in fact larger at Druids Run (2.84×10^{-5} and 1.12×10^{-5} for Druids Run and

Baisman Run, respectively), suggesting the difference in thickness accommodates the difference in transmissivity. The values are shown in Table 3.

We estimated drainable porosity and plant-available water content from literature values. We assumed drainable porosity was constant and equal to 0.25 at both sites, which is typical for materials with medium sand to medium gravel texture (Johnson, 1967). While drainable porosity is an important variable for regulating the degree to which the water table rises and falls in response to recharge, it has a relatively narrow range of possible values in comparison to other parameters, so a possible difference between the sites should not have a strong effect on our results. We estimated plant-available water content as 0.19 and 0.14 for Druids Run and Baisman Run respectively using characteristic values for our sites from the USDA Soil Survey.

Lastly, climatological variables were estimated using the approaches described in the methods section with weather station data and literature values. The relevant values are shown in Table 3.

Name	Symbol	Units	Druids Run	Baisman Run
Hydraulic conductivity	k_s	m/s	2.84e−5	1.12e−5
Permeable thickness	b	m	0.46	4.03
Plant-available water content	n_a	-	0.19	0.14
Drainable porosity	n_e	-	0.25	0.25
Mean storm duration	$\langle t_r \rangle$	s	1.02e4	1.02e4
Mean interstorm duration	$\langle t_b \rangle$	s	1.11e5	1.11e5
Mean storm depth	$\langle d_s \rangle$	m	4.50e−3	4.50e−3
Interstorm potential ET rate	pet	m/s	2.58e−8	2.58e−8

Table 3. All hydrological parameters needed to run DupuitLEM. The values for n_e , $\langle t_r \rangle$, $\langle t_b \rangle$, $\langle d_s \rangle$, and pet are identical at the two sites.

3.2.2 Geomorphic parameters

The uplift or baselevel change rate U is an important model parameter and is needed to obtain estimates of both the hillslope diffusivity D and the streampower incision coefficient K . Portenga et al. (2019) estimated the mean denudation rate of the Piedmont in the nearby Potomac River basin as 11.4 m/Myr (IQR 7.6 – 15.0) assuming an average rock density of 2700 kg/m³. We equated the denudation rate with uplift rate U , assuming geomorphic steady state. To quantify the uncertainty in U , and its contribution to the uncertainty in D and K , we estimated a probability distribution for U based on the box plot in Figure 4 of Portenga et al. (2019). The data did not appear particularly skewed, so we modeled denudation with a normal distribution, which we truncated to permit only positive values.

We estimated the diffusivity based on hilltop curvature, as presented in Equation 14. All the parameter values needed are shown in Table 4, and the distributions of the log of hilltop curvature are shown in Figure 10A. Hilltop curvature is quite similar at both sites. This is surprising because different processes likely contribute to diffusive transport at Druids Run versus Baisman Run. For example, freeze-thaw effects may be more important in the exposed, rocky soils at Druids Run, while treethrow may be more important in the forest-covered soils at Baisman Run. We estimated the diffusivity and its uncertainty by Monte Carlo simulation, sampling the distribution of U 10,000 times, and selecting 10,000 values from the hilltop curvature dataset independently with replacement. The distributions of diffusivity from the Monte Carlo simulation are shown in Fig-

ure 10B. The median diffusivity is $8.6\text{e-}3 \text{ m}^2/\text{yr}$ (IQR $4.4\text{e-}3 - 1.7\text{e-}2$) at Druids Run, and $9.3\text{e-}3 \text{ m}^2/\text{yr}$ (IQR $4.3\text{e-}3 - 1.9\text{e-}2$) at Baisman Run.

	$C_{HT} \text{ (m}^{-1}\text{)}$			$U \text{ (m/yr)}$		
	Med	LQ	UQ	Med	LQ	UQ
Druids Run	$-1.272\text{e-}3$	$-2.084\text{e-}3$	$-7.053\text{e-}4$	$1.193\text{e-}5$	$7.561\text{e-}6$	$1.495\text{e-}5$
Baisman Run	$-1.125\text{e-}3$	$-2.123\text{e-}3$	$-6.571\text{e-}4$	$1.193\text{e-}5$	$7.561\text{e-}6$	$1.495\text{e-}5$

Table 4. Hilltop curvature C_{HT} and uplift U for Baisman Run and Druids Run. Negative curvature indicates convexity. Uplift values are the same for both sites.

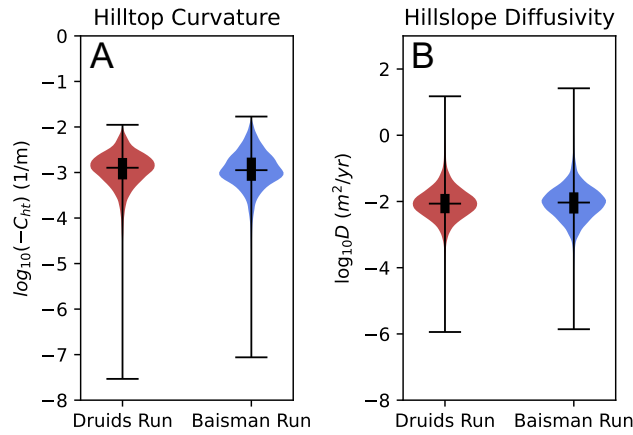


Figure 10. Violin plots of the log of hilltop curvature and log of hillslope diffusivity for Druids Run (A) and Baisman Run (B). Violin plots show the median, minimum, and maximum (horizontal lines) values and the interquartile range (wider vertical bar). Both distributions are similar, though Druids Run has slightly higher curvature, and therefore slightly lower diffusivity.

We calculated the streampower incision coefficient K using Equation 22 by estimating n , k_{sn} , and Q_{max}^* . We first conducted a χ -analysis of the channel networks of both sites to determine the streampower exponent n and then the appropriate steepness index k_{sn} . Lastly, we estimated the maximum dimensionless discharge Q_{max}^* based on available hydrologic data.

To calculate the optimal coordinate χ , we need to estimate the concavity index m/n (see Equation 20) for which the channel network collapses to a single line in χ -elevation space (Perron & Royden, 2013). We tried a range of values for the concavity index and determined that $m/n = 1/2$ produced a satisfactory collinearity of channels for both of the sites. Independently estimating the exponents m and n is challenging (Harel et al., 2016), so we chose the combination $m = 1/2$ and $n = 1$ for consistency with our prior modeling studies.

We determined k_{sn} from the slope of the relationship between χ and elevation for individual channel segments using the method described by S. M. Mudd et al. (2014). We estimated K using the segments that are above the 40th percentile of channel network drainage area, which are colored by k_{sn} in Figure 11A–B. We selected this drainage

area cutoff to isolate channel segments where Q^* is less likely to vary with distance downstream. We found that channel segments with smaller upslope areas were often less linear in χ -elevation space, which may indicate a change in Q^* with area. Figure 11C shows the distribution of k_{sn} values that meet these criteria. We found that k_{sn} was nearly twice as high at Druids Run, with a median of 2.774 (IQR 2.163 – 3.284), as Baisman Run, with a median of 5.23 (IQR 4.747 – 7.017).

	k_{sn} (m)			Exponents (-)		Runoff (-)
	Median	LQ	UQ	m	n	Q_{max}^*
Druids Run	2.774	2.163	3.284	0.5	1	0.3
Baisman Run	5.230	4.747	7.017	0.5	1	0.3

Table 5. Channel steepness index k_{sn} , streampower exponents, and maximum runoff rate Q_{max}^* for Baisman Run and Druids Run.

We estimated the maximum dimensionless discharge Q_{max}^* at Baisman Run as the long-term average runoff ratio $\langle Q \rangle / \langle P \rangle = 0.3$ (Cosans, 2022). From our short timeseries at Druids Run, we calculated a runoff ratio of 0.57. Because k_{sn} depends on the product of K and Q_{max}^* (Equation 21) in our model, these data suggest that the factor of two difference in k_{sn} between our sites could be due to the difference in the hydrology, expressed in Q_{max}^* , rather than a difference in material and geomorphic properties, expressed in K . While that would support our hypothesis, we will conservatively set $Q_{max}^* = 0.3$ for Druids Run as a first estimate, matching Baisman Run.

With all components of Equation 22 estimated, we used the same Monte Carlo procedure to calculate K and its uncertainty. Figure 11D shows that K is substantially higher at Druids Run than at Baisman Run when Q_{max}^* is set equal. The median at Druids Run is $1.34\text{e-}5 \text{ yr}^{-1}$ (IQR $8.24\text{e-}6 - 1.98\text{e-}5$), while at Baisman Run it is $6.49\text{e-}6 \text{ yr}^{-1}$ (IQR $3.83\text{e-}6 - 9.66\text{e-}6$). The full table of geomorphic parameters are shown in Table 6.

Name	Symbol	Units	Druids Run	Baisman Run
Uplift rate	U	m/yr	$1.143\text{e-}5$	$1.143\text{e-}5$
Hillslope diffusivity	D	m^2/yr	$8.611\text{e-}3$	$9.285\text{e-}3$
Streampower incision coefficient	K	1/yr	$1.334\text{e-}5$	$6.546\text{e-}6$
Contour length	v_0	m	30	30

Table 6. Geomorphic parameters needed to run DupuitLEM. We used the median value from the estimated parameter distributions for U , D , and K . The values for U and the characteristic contour length v_0 are identical at the two sites.

The difference in streampower incision coefficient between the two sites potentially confounds our interpretation of subsurface hydrologic controls on emergent hillslope length and hydrological function, assuming the difference is due to a contrast in material properties rather than hydrology. Our estimated subsurface hydrological variables support our perceptual model of how the sites should be different if they have coevolved with their hydrology; lower transmissivity at Druids Run should lead to more surface runoff and channel incision, and greater extent of variably saturated areas than the high transmissivity conditions at Baisman Run. However, a higher streampower incision coefficient may indicate that runoff is more effective at detaching and transporting sediment out of the watershed at Druids Run, which could also lead to closer spacing of channels and shorter hillslopes (Perron et al., 2008).

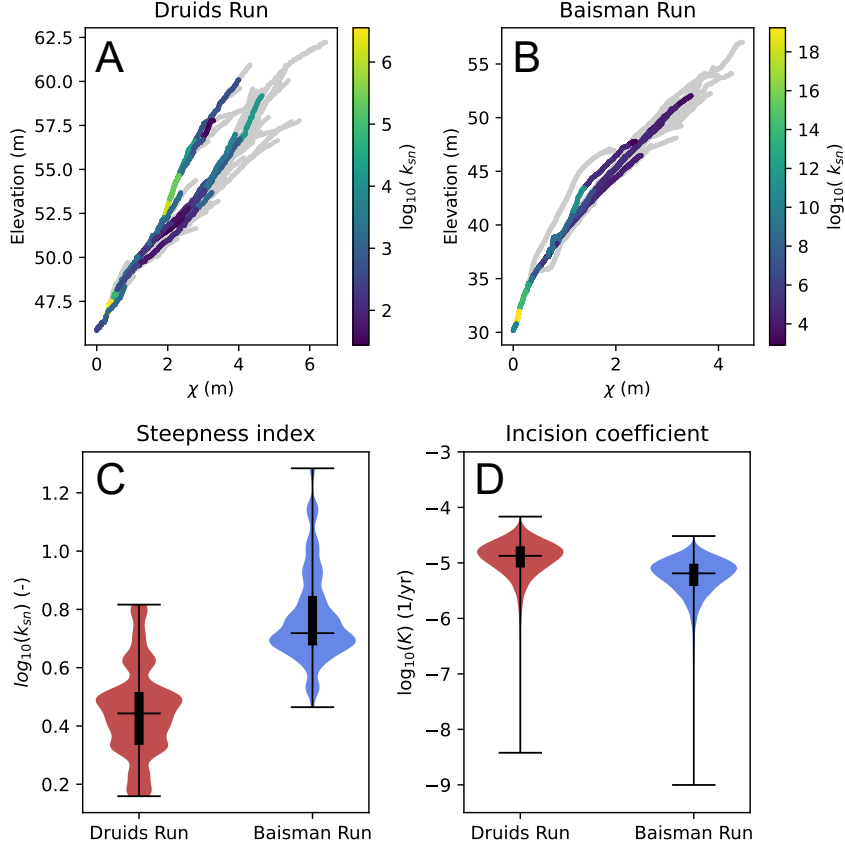


Figure 11. χ -elevation plots for Druids Run (A) and Baisman Run (B) for a concavity index $m/n = 0.5$. Channel segments are colored by their steepness index k_{sn} where the upslope area is greater than the 40th watershed area percentile, and are otherwise gray. (C) the distributions of k_{sn} for the segments colored in (A) and (B), showing generally higher channel steepness at Baisman Run than Druids Run. (D) distributions of the streampower incision coefficient K from Monte Carlo simulations. k_{sn} scales inversely with the erodibility, such that the streampower incision coefficient is lower at Baisman Run than Druids Run.

To test whether subsurface hydrology is necessary and sufficient for explaining the difference in variable source areas and hillslope length at the two sites, we ran four simulations, shown in Figure 12: two that represent our best estimates of hydrological and geomorphic parameters as described above (DR-DR, BR-BR), and two where we swapped the geomorphic parameters (DR-BR, BR-DR). Our best estimate cases helped discriminate how well DupuitLEM can capture landscape geomorphic and hydrologic dynamics at our sites. By comparing the best estimate simulations with simulations that have the same hydrological parameters but swapped geomorphic parameters, we determined whether geomorphic process rates alone explained the differences in morphology when the landscape coevolves with hydrology. Due to uncertainties in initial conditions and landscape history, we do not expect the simulation results to look exactly like Druids Run or Baisman Run. Instead, we compared them on the basis of aggregate properties including the hillslope length and relief, and saturation behavior. Beyond the direct site comparison, this approach also allows for exploration of topographic sensitivity to subsurface properties in a realistic region of the DupuitLEM parameter space.

		Hydrologic Variables (k_s, b, n_o)	
		Druids Run (DR)	Baisman Run (BR)
Geomorphic Variables (K, D)	DR	DR-DR	BR-DR
	BR	DR-BR	BR-BR

Figure 12. Four boxes indicating the four simulations we conducted. Colored boxes indicate the correctly matched hydrologic and geomorphic parameters, while white boxes indicate the ones in which the geomorphic variables are swapped. The listed hydrological and geomorphic variables are those that are varied, while all others are kept the same.

Lastly, we considered what happens when the differences in observed channel steepness were due to differences in runoff ratio (Q_{max}^*) rather than material properties (K). In our model formulation, determining the right value of Q_{max}^* should be an iterative process, in which the value of Q_{max}^* is estimated in order to determine erodibility, the model is run forward, the discharge and precipitation from the simulated landscape are used to recalculate Q_{max}^* , and then the streampower incision coefficient is adjusted accordingly. This would be repeated until the estimated Q_{max}^* value matches the value produced by the simulation. If there is a mismatch, the channel steepness of the modeled topography will be offset from that measured at the site. While we did not do a complete iterative solution, we did adjust Q_{max}^* and K according to the results of our first simulation.

3.3 Landscape evolution results

The landscape evolution model results showed subsurface hydrology has a significant effect on the morphology of emergent landscapes, and revealed the complexity of interactions between hydrologic and geomorphic processes. However, the model was unable to faithfully reproduce the hillslope length, relief, and (for Druids run particularly) important details of the hydrologic behavior.

We first simulated topography for the four cases presented in Figure 12, and analyzed the hillslope properties and persistence of saturated areas using the same crite-

ria as we used for the field sites. The only necessary difference was that we identified channel heads using a threshold on topographic curvature ($\nabla^2 z > 0.001$), because the DrE-ICH algorithm performed poorly on our model simulations, which are much lower resolution than the lidar-derived DEMs. Because the transmissivity is the primary difference in hydrological variables, we call the cases with hydrology like Druids Run (DR-DR and DR-BR) the low transmissivity cases, and cases with hydrology like Baisman Run (BR-BR and BR-DR) the high transmissivity cases.

The most striking pattern in the hillshades shown in Figure 13A is that the low transmissivity cases were substantially more dissected than the high transmissivity cases. DR-DR and DR-BR, the two cases with hydrological parameters estimated for Druids Run, have extensive fluvial dissection that extends onto hillslopes, which appears more extensive than we observed at Druids Run. However, the broad undissected hillslopes in BR-BR and BR-DR are similar to what we observed at Baisman Run. Despite some visual similarities, Figure 13B–C shows that BR-BR and BR-DR cases tended to overpredict hillslope length and relief. Also, contrary to our expectations, in the low transmissivity cases where the geomorphic properties have been swapped (DR-DR versus DR-BR), the difference in hillslope length and relief appeared to be comparable to the difference between Baisman Run and Druids Run (for a better view of length and relief at the field sites, see Figure 8). However, the presence of fluvial dissection broadly across these modeled topographies makes direct comparison with our field sites more difficult. In the high transmissivity cases, channels are clearly defined from hillslopes, but we have a smaller sample from which to derive metrics. Hillslope length and relief appear to be less sensitive to the difference in geomorphic variables than in the low transmissivity cases.

Swapping geomorphic parameters had a relatively minor effect on hydrological function. Figure 14A shows that simulations with swapped geomorphic parameters but the same hydrologic parameters have very similar saturated area patterns, whereas there is a substantial difference between simulations that have different hydrologic parameters. The low transmissivity cases have large variably saturated areas that extend onto hilltops, as at Druids Run, though there are no hilltops that are classified as dry in the low transmissivity cases. They also show more persistent saturation in valley bottoms and zero-order basins than observed in Druids Run (Figure 14A–B). The saturated areas modeled in the high transmissivity cases look very similar to those observed at Baisman Run, where there is persistent saturation in valley bottoms and dry hilltops. Some channel heads near the domain boundary of BR-BR even show wider seep-like channel heads, which may be analogous to the saturated headwaters and springs seen at Baisman Run. The fractional saturated areas are similar to those observed at the sites as well (Figure 14B).

Next we examined the emergent runoff ratio and adjusted the fluvial parameters to account for the difference between the runoff ratio and the initial estimate of Q_{max}^* . The emergent runoff ratio for the high transmissivity cases were 0.33 and 0.32 for BR-BR and BR-DR respectively, which were very close to our initial estimate of 0.3, which was the observed runoff ratio at Baisman Run. The difference in geomorphic parameters had little effect on emergent runoff ratio in these cases. In the low transmissivity cases, the runoff ratio was significantly higher than our initial estimate of 0.3. We found runoff ratios of 0.86 and 0.81 for DR-DR and DR-BR respectively. These values are again not highly sensitive to the difference in geomorphic parameters, but both are substantially higher than our initial estimate, and higher than our field estimate of 0.57 for Druid Run. However, this is consistent with our observation that DR-DR and DR-BR have much more extensive saturated areas than Druids Run. These higher runoff ratios suggest that we should increase estimated Q_{max}^* , and therefore decrease the estimated K at Druids Run. If we increase Q_{max}^* to 0.6, the corresponding K values is $6.68e-6 \text{ yr}^{-1}$, which is within 3% of the K value we estimated for Baisman Run. The geomorphic results of this increase are shown in Figure 15. The hydrologic effect of this increase is minimal, as shown in Figure S2.

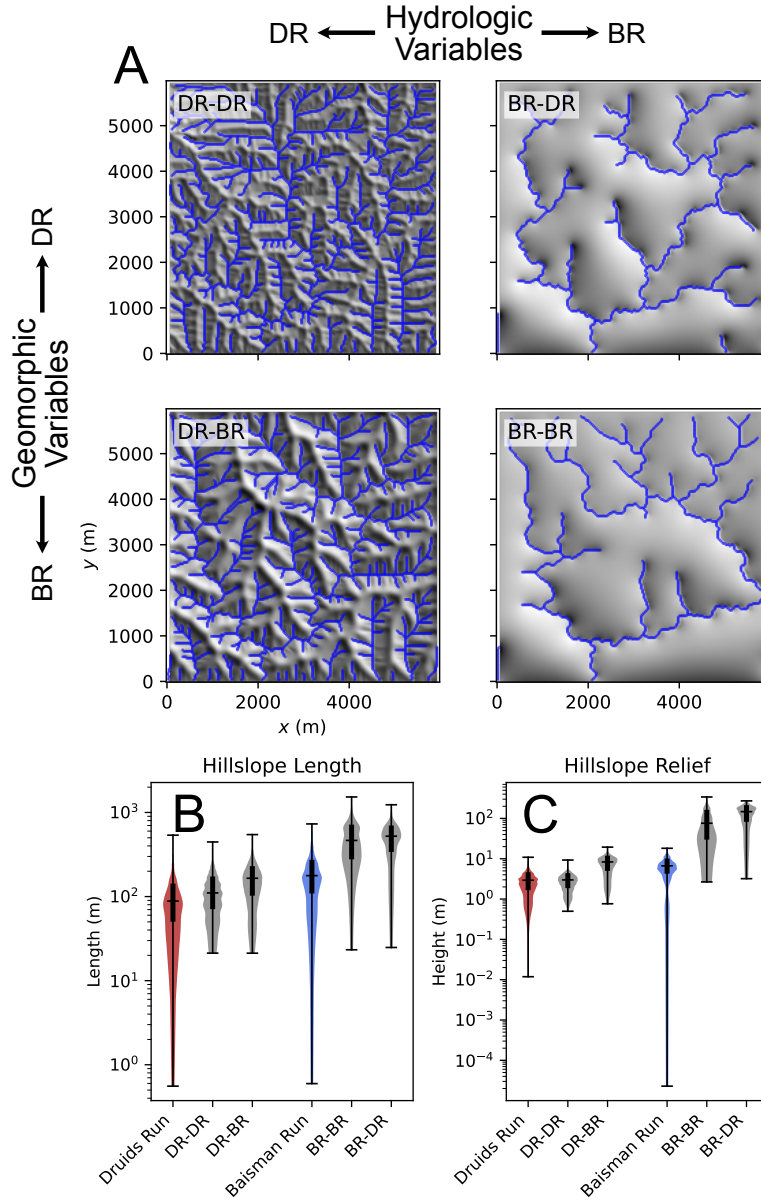


Figure 13. (A) Hillshades of model results in the same configuration as shown in Figure 12. Dissection is substantially higher in cases with Druids Run hydrological variables than Baisman Run hydrological variables. (B, C) Log-scaled violin plots of hillslope length and relief, comparing the field data (labelled “Druids Run” and “Baisman Run”) to the four modeled cases. Horizontal lines represent the maximum and minimum values, while the vertical bar represents the interquartile range.

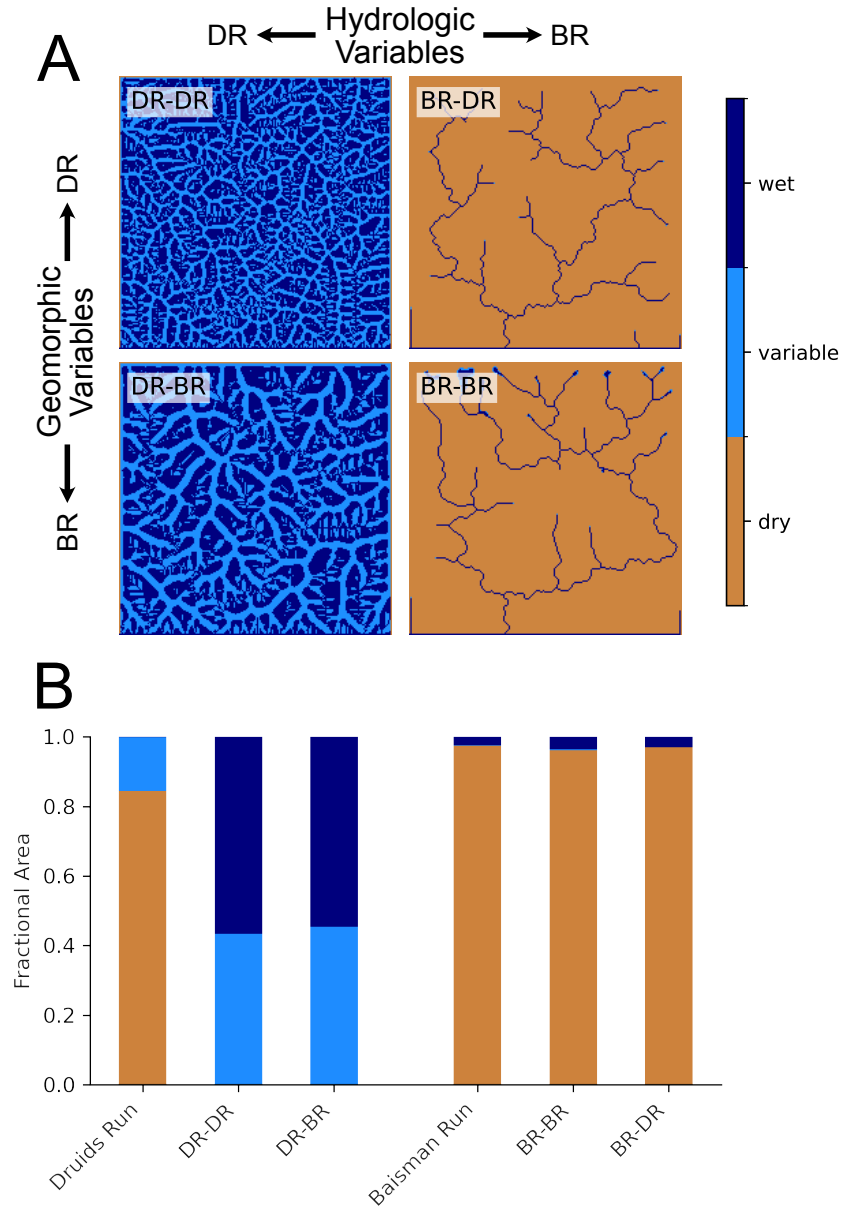


Figure 14. (A) Map view of saturated area classes for model results in the same configuration as shown in Figure 12 and Figure 13A. Saturated area behavior is not highly sensitive to swapping geomorphic variables, while it is sensitive to swapping hydrological variables. (B) Fractional area that is classified as wet, variable, and saturated based on field data (labelled “Druids Run” and “Baisman Run”) and the four modeled cases. Cases that have the hydrological variables associated with Baisman Run appear similar to the field characteristics of Baisman Run. Cases that have the hydrological variables associated with Druids Run show more persistent saturation than the field characteristics of Druids Run.

Adjusting the streampower incision coefficient for differences in Q_{max}^* nearly eliminates the difference in emergent morphology and hydrology between cases with swapped geomorphic parameters. The hydrological function of the landscapes is very similar when geomorphic parameters are swapped, which is expected given that there was little difference in hydrological function between the original cases with swapped geomorphic parameters. The emergent runoff ratio for DR-DR is now 0.78, which is slightly lower than we calculated previously. The modeled topography looks very similar when geomorphic parameters are swapped, and distributions of hillslope length and relief are nearly identical (Figure 15). At least within the context of our model, this suggests that differences in geomorphic parameters are not sufficient to explain the differences between the sites. The results suggest that the difference in morphology between Druids Run and Baisman Run is strongly affected by the difference in their subsurface hydrology, as (1) the difference in transmissivity changes the extent of saturated areas and surface water on the landscape, which changes the proportion of the landscape that experiences fluvial erosion, and (2) higher runoff ratios increase the efficiency of water-driven sediment transport in areas where there is saturation, which further incises the landscape.

Our results also showed that there is more work to do to understand the controls on the geomorphic evolution of our sites. For instance, adjusting Q_{max}^* did not bring us closer to the true hillslope length and relief. Figure 16 shows how the true cases DR-DR and BR-BR compare to the hillslope length and relief of Druids Run and Baisman Run, respectively. The number in parentheses following the model label is the estimated value of Q_{max}^* . The values of hillslope length and relief from simulation DR-DR (0.6) were farther from the true values at Druids Run than those from simulation DR-DR (0.3). At the same time, we know that the channel steepness k_{sn} from the simulation DR-DR (0.3) will not match k_{sn} of Druids Run, because we overestimated the streampower incision coefficient K relative to the emergent value of Q_{max}^* . More work is needed to understand both the possible difference in other parameters (e.g., the denudation rate) and limitations of model structure for capturing our sites, but it is clear that the difference in the hydrology of the sites is an important component of their geomorphic evolution.

4 Discussion

4.1 The expression of subsurface hydrology in landscape evolution

Previous work on the role of transmissivity in topographic evolution (Luijendijk, 2022; Litwin et al., 2022, 2024) is a logical extension of the hydrological study of runoff generation, as sediment transport is an important consequence of runoff generation. It has only recently received attention, in part because considering the long-term effects of this coevolution is computationally intensive, and in part because it relies on subsurface properties that are hard to estimate. Available models also lack critical aspects of channel head formation, which would themselves require more thorough treatment of the conversion of rock to regolith (see Section 4.2.2). As a result, landscape evolution models typically select the minimally-complex model needed to explain their observations. As a result, they have often excluded subsurface hydrology, despite the widespread importance of subsurface flow for runoff generation (Wu et al., 2021). We have shown here that subsurface hydrology may be indispensable for understanding the evolution of some landscapes. The importance of subsurface runoff generation for a particular application of a landscape evolution model is dependent on the geologic and climatic setting, but also on the scale of interest. Studies focusing on watershed scales of 1-10s of kilometers may find that capturing subsurface flow is essential, while these details may be less important in the evolution of entire orogens, where the length of subsurface flow paths relevant to runoff generation is shorter than the scales of geomorphic interest.

We showed strong sensitivity of topography to subsurface hydrology for reasonable combinations of parameters, but also showed that there were limitations to how realis-

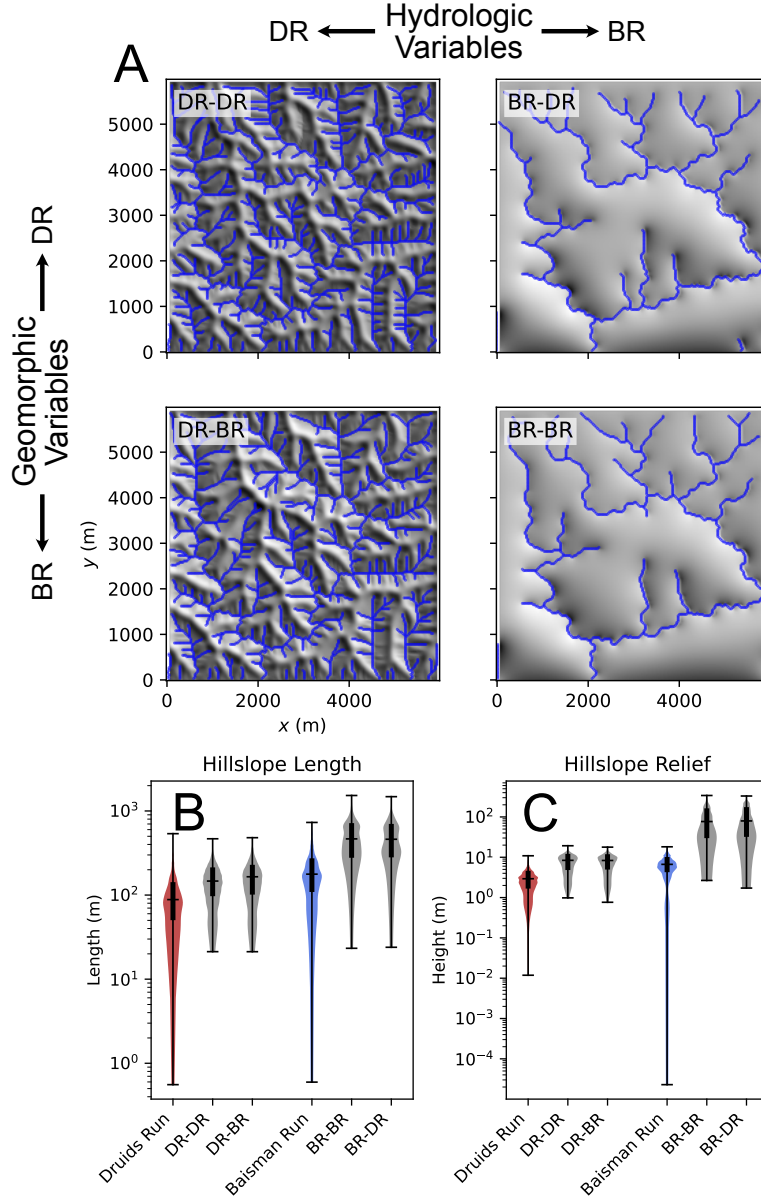


Figure 15. (A) Hillshades of model results in the same configuration as shown in Figure 12, only $Q_{max}^* = 0.6$ was used to determine the streampower incision coefficient for cases with Druids Run geomorphic variables. Visual comparison of results suggests that the difference in hydrology between the two sites is the primary control on emergent morphology. (B, C) Violin plots of hillslope length and relief, comparing the field data (labelled “Druids Run” and “Baisman Run”) to the four modeled cases. There is little difference between simulations with swapped geomorphic variables (comparing down columns), while there is still substantial sensitivity to swapped hydrological variables (compare across rows). All four modeled cases still have length and relief greater than those observed in the field.

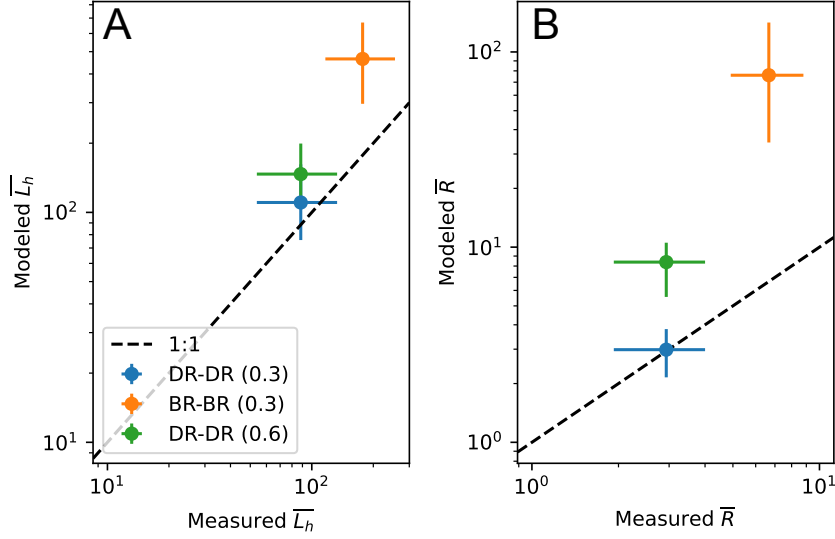


Figure 16. Modeled versus observed hillslope length (A) and hillslope relief (B). Results are only shown for the true cases (not the swapped parameter cases). The number following the simulation name is the value of Q_{max}^* . For Druids Run, simulations using both the original and updated estimates of Q_{max}^* are shown. The points are median values, and the error bars show the interquartile range.

tically DupuitLEM can capture our sites. We were able to make both of these assessments in part because we had hydrologic as well as geomorphic observations. While many studies have sought to test the sensitivity of landscape morphology to climate (e.g., Ferrier et al., 2013; Adams et al., 2020; Zavala et al., 2020), hydrological field data can reveal functional differences between sites due to subsurface properties that would be indistinguishable based on climate alone. Measurements of the location and magnitude of runoff and erosion are likely the most relevant variables for such assessments. Discharge records are widely available and can provide some indication on runoff generation mechanisms (McMillan, 2020). The addition of sediment concentration timeseries can enrich discharge timeseries to provide a stronger link between runoff generation and erosion (Tolorza et al., 2014). When possible, observations of runoff on foot, or remotely with cameras or satellite platforms (Godsey & Kirchner, 2014; Antonelli et al., 2020; Dralle et al., 2023; Harrison et al., 2020) can provide valuable comparisons to basin-integrated timeseries. Geomorphic proxies may also be useful. Rossi et al. (2020) found that bedrock exposure, as a proxy for low subsurface storage and infiltration capacity, explained variation in extreme runoff events better than variation in precipitation across an elevation gradient in the Colorado Front Range. Combinations of discharge, topographic analysis, and cosmogenic erosion rates have also allowed new examinations of channel head forming mechanisms that could be useful for informing future modelling (Harrison et al., 2020).

4.2 Parameter estimation and limits of DupuitLEM

While our results provide evidence for a critical link between subsurface hydrology and landscape evolution, there are clear discrepancies between the characteristics of Baisman Run and Druids Run that we observed and those we were able to model with DupuitLEM. Some of these discrepancies could be due to our choice of model parameters, while others appear to be structural limitations of DupuitLEM.

808 4.2.1 *Parameter uncertainty*

809 Our results here and in prior studies (Litwin et al., 2022, 2024) demonstrate that
 810 emergent topography and hydrology are highly sensitive to transmissivity, so the accu-
 811 racy of the transmissivity estimate is likely a factor in model-data discrepancies. Our
 812 novel approach to estimate transmissivity relied on topographic index as a measure of
 813 hydrological similarity (O’Loughlin, 1986; Beven & Kirkby, 1979). However, our results
 814 showed that topographic index and discharge, when combined in Equation 7, were only
 815 modestly good predictors of saturated area (Figure 9). Furthermore, topographic index
 816 is a resolution-dependent quantity (Zhang & Montgomery, 1994), which means that the
 817 resulting transmissivity that we calculate also depends on DEM resolution. While ac-
 818 counting for this effect is unlikely to change the relative magnitudes of transmissivity be-
 819 tween the sites, it may change the estimated values. This was a problem with calibrated
 820 transmissivities in TOPMODEL as well (Beven, 1997), so some of the strategies that have
 821 been devised to reduce the scale dependence in that context (e.g., Saulnier et al., 1997)
 822 may be useful for improving our transmissivity estimates as well.

823 Our model results also showed that hillslope length and relief were too large in the
 824 simulated landscapes regardless of transmissivity. This could suggest that the relative
 825 magnitude of hillslope diffusivity to the fluvial erosion efficiency is too large (Perron et
 826 al., 2008; Theodoratos et al., 2018). Our modelled cases are generally able to reproduce
 827 observed hilltop curvature (Figure S3A), which suggests that the diffusivity is not the
 828 primary issue. Modelled channel steepness, however, is systematically larger than the
 829 channels from which the parameters were defined (Figure S3B). One likely issue that could
 830 explain this discrepancy arises from using K estimates from 1D channel profiles in a 2D
 831 model. Hillslopes in the 2D model contribute material to valleys that rivers must remove.
 832 This decreases their erosional efficiency compared to what is expected when estimating
 833 K from a 1D profile in which the river only needs to erode at a rate U (Equation 16).
 834 This topic requires further exploration than can be accommodated here, and will be cov-
 835 ered in future work.

836 4.2.2 *Process uncertainty*

837 While there are limitations to our ability to estimate transmissivity and other pro-
 838 cess rates, we know that some key hydrological and geomorphic processes and features
 839 are missing from our model. These may be the cause of the model’s inability to accu-
 840 rately reproduce the length and relief at each site. DupuitLEM was designed to be a min-
 841 imally complex representation of coupled hydrology and landscape evolution in humid
 842 upland environments, and thus necessarily left many processes out that are relevant to
 843 the particular sites we have discussed here.

844 A key hydrological limitation of our model is in the routing of surface water. It is
 845 challenging to balance flow convergence and divergence in a single efficient algorithm (Pelletier,
 846 2010). We use the D8 flow algorithm (O’Callaghan & Mark, 1984), which directs all flow
 847 at a point to a single downslope node. This may be a key limitation for comparison with
 848 Druids Run, where we observed saturation and runoff on divergent hillslopes. Our sim-
 849 plifications in our vadose zone model also prevent evaporation or transpiration of wa-
 850 ter from the saturated zone. Including it would decrease the proportion of the water-
 851 shed that stays saturated during interstorm periods and decrease antecedent wetness when
 852 storms arrive.

853 Our subsurface model was also limited to be spatially uniform and homogeneous.
 854 We know this is not the case. In Baisman Run, deeply weathered zones under hillslopes
 855 delay the arrival of hillslope water to streams and support baseflow, while a relatively
 856 shallow subsurface in valley bottoms may increase the likelihood of overland flow in the
 857 channels (Cosans, 2022; St. Clair et al., 2015). This pattern could increase flow persis-
 858 tence and drainage dissection relative to a uniform subsurface. In contrast, very thin soils

on hillslopes at Druids Run allow saturation and overland flow to occur frequently, while a more permeable valley bottom may increase the subsurface conveyance in valleys relative to the amount of water that remains after storms. Depending on how the riparian area is connected to the stream, it may also store more water that can be slowly released during interstorm periods. These patterns could increase or decrease saturated areas and drainage dissection, depending on the extent of the riparian aquifer and its stream connection.

In addition to shaping subsurface structure, weathering can also result in significant chemical denudation. DupuitLEM, like many geomorphic models, only treats physical erosion. Cleaves et al. (1974) studied the denudation of Pond Branch (a subwatershed of Baisman Run) and a small watershed on the Soldiers Delight Ultramafite that is south of our site. On the basis of a geochemical mass balance, they estimated that chemical weathering was responsible for approximately 90% of denudation in Soldiers Delight at present, while it was responsible for approximately 50% of denudation at Pond Branch. This could suggest a significant difference in interpretation of morphologic differences. We discuss this further in A.

There are also limitations to the style of erosion considered by the model. In environments with humid climates and crystalline bedrock, seepage erosion at springs may play an important role in channel network evolution, given that shear stress at channel heads may not generally be high enough to incise bedrock alone (Dunne, 1990, 1980). This could help explain why the drainage density in our model parameterized for Baisman Run is higher than that in the real watershed. A more thorough treatment of this process would also require more consideration for weathering, which must ultimately supply material that can be transported at the low discharge rates found at channel heads. Despite lacking this complexity, our model is still able to simulate some spring-like features that are characteristic of Baisman Run. This suggests a degree of flexibility of the streampower law, when coupled with the right discharge function.

5 Conclusions

The analysis of the two study sites and modeling with DupuitLEM presented here support the idea that subsurface transmissivity is a major control on not only the hydrologic function of humid, soil-mantled landscapes, but also on their morphology. We framed this paper with two hypotheses about how the morphology and hydrological function of two landscapes should be different, informed by understanding (gleaned from previous modeling studies) of how the subsurface could affect the coevolution of runoff and topography. From field data, we found that both the hydrological function and morphology aligned with our predictions; Druids Run, which has a thin permeable subsurface, had more extensive variably saturated areas, more variable effective area contributing runoff, and shorter hillslopes than Baisman Run, which has a deep permeable subsurface. A novel use of topography, saturation and discharge observations further showed that the transmissivity was substantially higher at Baisman Run than Druids Run.

We parameterized a coupled groundwater landscape evolution model for each site using field observations, topographic analysis, and literature values, and ran the model to geomorphic steady state. We were able to simulate the broad dry hillslopes and persistently saturated valley bottoms at Baisman Run, but substantially overpredicted saturation at Druids Run. The model correctly predicted that hillslope length and relief would be substantially larger in the high-transmissivity site (Baisman Run), but was unable to reproduce the actual hillslope length and relief: at both sites it predicted longer and higher hillslopes. These differences may be due to issues related to uncertainty and biases in parameter estimation, and to inadequate representation of the actual geomorphic processes operating at each site. However, the difference in geomorphic process rates was not sufficient to explain the between-site difference in hillslope length or hydrolog-

ical function, suggesting that the morphologic differences between the sites could reasonably be attributed to subsurface transmissivity.

Appendices

A Geomorphic contrasts based on chemical denudation

Some recent work begins to provide a framework for understanding morphologic effects of chemical denudation. Ben-Asher et al. (2019) introduced a modification of the hillslope mass balance that includes chemical denudation in the form of a chemical depletion fraction (CDF). They showed that curvature should be reduced as the ratio of chemical to total denudation increases, assuming a constant hillslope diffusivity. Marcon (2019) applied this principle to several hillslopes on contrasting lithologies across the Piedmont, including sites on schist and serpentine bedrock. They found decreasing hilltop curvature with increasing CDF, where serpentine sites had the highest CDF and lowest hilltop curvatures. At our sites we found virtually no difference in hilltop curvature between lithologies. If the total denudation rate at both sites is indeed very similar, but chemical denudation is dramatically different, we are left with the conclusion that the identical curvature is a coincidence that arises from higher hillslope diffusivity D at Druids Run than Baisman Run. Further research, including updated denudation estimates specific to our sites, would be needed to draw further conclusions on chemical denudation rates and geomorphic consequences at our sites.

6 Open Research

All original data, model output, and scripts needed to process data and generate figures are archived on Zenodo (Litwin & Harman, 2024). The Python package DupuitLEM v1.1 (Litwin et al., 2023) contains the models and scripts used to generate and post-process the model output. Landlab v2.0 (Barnhart et al., 2020) is a core dependency of DupuitLEM.

Acknowledgments

This work was supported by National Science Foundation grants EAR-2012264 and EAR-1654194. Model simulations were carried out at the Advanced Research Computing at Hopkins (ARCH) core facility (rockfish.jhu.edu), which is supported by the National Science Foundation (NSF) grant number OAC-1920103. We appreciate help in the field from Joseph Stanley. We thank Tom Dunne, Gordon Grant, and an anonymous reviewer for comments that led to significant improvements in this manuscript.

References

- Adams, B. A., Whipple, K. X., Forte, A. M., Heimsath, A. M., & Hodges, K. V. (2020). Climate controls on erosion in tectonically active landscapes. *Science Advances*, 6(42), eaaz3166. (Publisher: American Association for the Advancement of Science) doi: 10.1126/sciadv.aaz3166
- Antonelli, M., Glaser, B., Teuling, A. J., Klaus, J., & Pfister, L. (2020). Saturated areas through the lens: 1. Spatio-temporal variability of surface saturation documented through thermal infrared imagery. *Hydrological Processes*, 34(6), 1310–1332. doi: 10.1002/hyp.13698
- Barnhart, K. R., Hutton, E. W. H., Tucker, G. E., Gasparini, N. M., Istanbuluoglu, E., Hobley, D. E. J., . . . Bandaragoda, C. (2020). Short communication: Landlab v2.0: A software package for Earth surface dynamics. *Earth Surface Dynamics*, 8(2), 379–397. doi: 10.5194/esurf-8-379-2020

- 954 Bazilevskaya, E., Lebedeva, M., Pavich, M., Rother, G., Parkinson, D. Y., Cole, D.,
 955 & Brantley, S. L. (2013). Where fast weathering creates thin regolith and slow
 956 weathering creates thick regolith. *Earth Surface Processes and Landforms*,
 957 38(8), 847–858. doi: 10.1002/esp.3369
- 958 Ben-Asher, M., Haviv, I., Roering, J. J., & Crouvi, O. (2019). The potential influ-
 959 ence of dust flux and chemical weathering on hillslope morphology: Convex
 960 soil-mantled carbonate hillslopes in the Eastern Mediterranean. *Geomorphol-
 961 ogy*, 341, 203–215. doi: 10.1016/j.geomorph.2019.05.021
- 962 Beven, K. (1997). TOPMODEL: A critique. *Hydrological Processes*, 11(9), 1069–
 963 1085. doi: 10.1002/(SICI)1099-1085(199707)11:9<1069::AID-HYP545>3.0.CO;
 964 2-O
- 965 Beven, K., & Kirkby, M. (1979). A physically based, variable contributing area
 966 model of basin hydrology. *Hydrological Sciences Bulletin*, 24(1), 43–69. doi: 10
 967 .1080/02626667909491834
- 968 Brantley, S. L., Eissenstat, D. M., Marshall, J. A., Godsey, S. E., Balogh-Brunstad,
 969 Z., Karwan, D. L., . . . Weathers, K. C. (2017). Reviews and syntheses: On
 970 the roles trees play in building and plumbing the critical zone. *Biogeosciences*,
 971 14(22), 5115–5142. doi: 10.5194/bg-14-5115-2017
- 972 Cleaves, E. T. (1989). Appalachian Piedmont landscapes from the Permian to the
 973 Holocene. *Geomorphology*, 2(1), 159–179. doi: 10.1016/0169-555X(89)90010
 974 -X
- 975 Cleaves, E. T., Fisher, D. W., & Bricker, O. P. (1974). Chemical Weathering of Ser-
 976 pentinite in the Eastern Piedmont of Maryland. *GSA Bulletin*, 85(3), 437–444.
 977 doi: 10.1130/0016-7606(1974)85<437:CWOSIT>2.0.CO;2
- 978 Cleaves, E. T., Godfrey, A. E., & Bricker, O. P. (1970). Geochemical Balance of
 979 a Small Watershed and Its Geomorphic Implications. *GSA Bulletin*, 81(10),
 980 3015–3032. doi: 10.1130/0016-7606(1970)81[3015:GBOASW]2.0.CO;2
- 981 Clubb, F. J., Mudd, S. M., Milodowski, D. T., Hurst, M. D., & Slater, L. J. (2014).
 982 Objective extraction of channel heads from high-resolution topographic data.
 983 *Water Resources Research*, 50(5), 4283–4304. doi: 10.1002/2013WR015167
- 984 Collins, D. B. G., & Bras, R. L. (2010). Climatic and ecological controls of equi-
 985 librium drainage density, relief, and channel concavity in dry lands. *Water Re-
 986 sources Research*, 46(4). doi: 10.1029/2009WR008615
- 987 Cosans, C. L. (2022). *Landscape Structure, Flow Path, and Transport Co-Evolution
 988 in the Deeply Weathered Piedmont* (Thesis). Johns Hopkins University.
- 989 Crowley, W. P., Reinhardt, J., & Cleaves, E. T. (1975). *Geologic map of the Cock-
 990 eysville quadrangle* (QA-3 ed.). Baltimore, Maryland: Maryland Geological
 991 Survey.
- 992 Dralle, D. N., Lapidus, D. A., Rempe, D. M., & Hahm, W. J. (2023). Mapping
 993 Surface Water Presence and Hyporheic Flow Properties of Headwater Stream
 994 Networks With Multispectral Satellite Imagery. *Water Resources Research*,
 995 59(9), e2022WR034169. doi: 10.1029/2022WR034169
- 996 Dunne, T. (1980). Formation and controls of channel networks. *Progress in Physical
 997 Geography: Earth and Environment*, 4(2), 211–239. (Publisher: SAGE Publi-
 998 cations Ltd) doi: 10.1177/030913338000400204
- 999 Dunne, T. (1990). Chapter 1. Hydrology mechanics, and geomorphic implications
 1000 of erosion by subsurface flow. In *Geological Society of America Special Papers*
 1001 (Vol. 252, pp. 1–28). Geological Society of America. doi: 10.1130/SPE252-p1
- 1002 Eagleson, P. (1978). Introduction to Water Balance Dynamics. *Water Resources Re-
 1003 search*, 14(5), 705–712. doi: 10.1016/j.compchemeng.2012.11.011
- 1004 Ferrier, K. L., Huppert, K. L., & Perron, J. T. (2013). Climatic control of bedrock
 1005 river incision. *Nature*, 496(7444), 206–209. (Publisher: Nature Publishing
 1006 Group) doi: 10.1038/nature11982
- 1007 Godsey, S. E., & Kirchner, J. W. (2014). Dynamic, discontinuous stream net-
 1008 works: Hydrologically driven variations in active drainage density, flowing

- channels and stream order. *Hydrological Processes*, 28(23), 5791–5803. doi: 10.1002/hyp.10310
- Grieve, S. W., Mudd, S. M., & Hurst, M. D. (2016). How long is a hillslope? *Earth Surface Processes and Landforms*, 41(8), 1039–1054. doi: 10.1002/esp.3884
- Guice, G. L., Ackerson, M. R., Holder, R. M., George, F. R., Browning-Hanson, J. F., Burgess, J. L., ... Viete, D. R. (2021). Suprasubduction zone ophiolite fragments in the central Appalachian orogen: Evidence for mantle and Moho in the Baltimore Mafic Complex (Maryland, USA). *Geosphere*, 17(2), 561–581. doi: 10.1130/GES02289.1
- Harel, M. A., Mudd, S. M., & Attal, M. (2016). Global analysis of the stream power law parameters based on worldwide ^{10}Be denudation rates. *Geomorphology*, 268, 184–196. doi: 10.1016/j.geomorph.2016.05.035
- Harrison, E. J., Brocard, G. Y., Gasparini, N. M., Lyons, N. J., & Willenbring, J. K. (2020). Seepage erosion in the Luquillo Mountains, Puerto Rico, relict landscapes. *Journal of Geophysical Research: Earth Surface*, 125(6), e2019JF005341. doi: 10.1029/2019JF005341
- Hewlett, J. D., & Hibbert, A. R. (1967). Factors affecting the response of small watersheds to precipitation in humid areas. In *Int. Symp. Forest Hydrology*. doi: 10.1177/0309133309338118
- Horton, R. E. (1945). Erosional development of streams and their drainage basins; hydrophysical approach to quantitative morphology. *GSA Bulletin*, 56(3), 275–370. doi: 10.1130/0016-7606(1945)56[275:EDOSAT]2.0.CO;2
- Hurst, M. D., Mudd, S. M., Walcott, R., Attal, M., & Yoo, K. (2012). Using hilltop curvature to derive the spatial distribution of erosion rates. *Journal of Geophysical Research: Earth Surface*, 117(F2), n/a–n/a. doi: 10.1029/2011jf002057
- Jencso, K. G., & McGlynn, B. L. (2011). Hierarchical controls on runoff generation: Topographically driven hydrologic connectivity, geology, and vegetation. *Water Resources Research*, 47(11). doi: 10.1029/2011WR010666
- Johnson, A. (1967). *Specific yield: Compilation of specific yields for various materials* (USGS Numbered Series No. 1662-D). Washington, D.C.: U.S. Government Printing Office. doi: 10.3133/wsp1662D
- Litwin, D. G., Barnhart, K. R., Tucker, G. E., & Harman, C. J. (2023). *DupuitLEM: groundwater landscape evolution with landlab [software]*. Zenodo. doi: 10.5281/zenodo.7620978
- Litwin, D. G., & Harman, C. J. (2024). *Data and model output for "Evidence of subsurface control on the coevolution of hillslope morphology and runoff generation" [Dataset]*. Zenodo. doi: 10.5281/zenodo.10624746
- Litwin, D. G., Tucker, G. E., Barnhart, K. R., & Harman, C. J. (2022). Groundwater affects the geomorphic and hydrologic properties of coevolved landscapes. *Journal of Geophysical Research: Earth Surface*, 127(1), e2021JF006239. doi: 10.1029/2021JF006239
- Litwin, D. G., Tucker, G. E., Barnhart, K. R., & Harman, C. J. (2024). Catchment coevolution and the geomorphic origins of variable source area hydrology. *Water Resources Research*, 60(6), e2023WR034647. doi: 10.1029/2023WR034647
- Luijendijk, E. (2022). Transmissivity and groundwater flow exert a strong influence on drainage density. *Earth Surface Dynamics*, 10(1), 1–22. doi: 10.5194/esurf-10-1-2022
- Luo, W., Jasiewicz, J., Stepinski, T., Wang, J., Xu, C., & Cang, X. (2016). Spatial association between dissection density and environmental factors over the entire conterminous United States. *Geophysical Research Letters*, 43(2), 692–700. doi: 10.1002/2015GL066941
- Marcon, V. (2019). *The effect of lithology on (bio) geochemical weathering: sandstone to serpentinite* (Unpublished doctoral dissertation). The Pennsylvania State University, State College, PA.

- McMillan, H. (2020). Linking hydrologic signatures to hydrologic processes: A review. *Hydrological Processes*, 34(6), 1393–1409. doi: 10.1002/hyp.13632
- Mudd, S., Clubb, F., Grieve, S., Milodowski, D., Gailleton, B., Hurst, M., . . . Hutton, E. (2022). *LSDTopotools/LSDTopoTools2: LSDTopoTools2 v0.7*. Zenodo. doi: 10.5281/ZENODO.3245040
- Mudd, S. M., Attal, M., Milodowski, D. T., Grieve, S. W. D., & Valters, D. A. (2014). A statistical framework to quantify spatial variation in channel gradients using the integral method of channel profile analysis. *Journal of Geophysical Research: Earth Surface*, 119(2), 138–152. doi: 10.1002/2013JF002981
- NOAA. (2024). *NOAA atlas 14 point precipitation frequency estimates: MD*. Retrieved 2024-01-11, from https://hdsc.nws.noaa.gov/pfds/pfds_map_cont.html?bkmrk=md
- O’Callaghan, J. F., & Mark, D. M. (1984). The extraction of drainage networks from digital elevation data. *Computer Vision, Graphics, & Image Processing*. doi: 10.1016/S0734-189X(84)80011-0
- O’Loughlin, E. M. (1986). Prediction of Surface Saturation Zones in Natural Catchments by Topographic Analysis. *Water Resources Research*, 22(5), 794–804.
- Pavich, M. J. (1989). Regolith residence time and the concept of surface age of the Piedmont “Peneplain”. *Geomorphology*, 2(1), 181–196. doi: 10.1016/0169-555X(89)90011-1
- Pelletier, J. D. (2010). Minimizing the grid-resolution dependence of flow-routing algorithms for geomorphic applications. *Geomorphology*, 122(1), 91–98. doi: 10.1016/j.geomorph.2010.06.001
- Perron, J. T., Dietrich, W. E., & Kirchner, J. W. (2008). Controls on the spacing of first-order valleys. *Journal of Geophysical Research: Earth Surface*, 113(4), 1–21. doi: 10.1029/2007JF000977
- Perron, J. T., & Royden, L. (2013). An integral approach to bedrock river profile analysis. *Earth Surface Processes and Landforms*, 38(6), 570–576. doi: 10.1002/esp.3302
- Portenga, E. W., Bierman, P. R., Trodick, C. D., Jr., Greene, S. E., DeJong, B. D., Rood, D. H., & Pavich, M. J. (2019). Erosion rates and sediment flux within the Potomac River basin quantified over millennial timescales using beryllium isotopes. *GSA Bulletin*, 131(7-8), 1295–1311. doi: 10.1130/B31840.1
- Prancevic, J. P., & Kirchner, J. W. (2019). Topographic controls on the extension and retraction of flowing streams. *Geophysical Research Letters*, 0(0). doi: 10.1029/2018GL081799
- Putnam, S. M. (2018). *The influence of landscape structure on storage and stream-flow generation in a Piedmont catchment* (Thesis). Johns Hopkins University.
- Roering, J. J., Perron, J. T., & Kirchner, J. W. (2007). Functional relationships between denudation and hillslope form and relief. *Earth and Planetary Science Letters*, 264(1), 245–258. doi: 10.1016/j.epsl.2007.09.035
- Rossi, M. W., Anderson, R. S., Anderson, S. P., & Tucker, G. E. (2020). Orographic Controls on Subdaily Rainfall Statistics and Flood Frequency in the Colorado Front Range, USA. *Geophysical Research Letters*, 47(4), e2019GL085086. doi: 10.1029/2019GL085086
- Sangireddy, H., Carothers, R. A., Stark, C. P., & Passalacqua, P. (2016). Controls of climate, topography, vegetation, and lithology on drainage density extracted from high resolution topography data. *Journal of Hydrology*, 537, 271–282. doi: 10.1016/j.jhydrol.2016.02.051
- Sauer, V. B., & Meyer, R. W. (1992). *Determination of error in individual discharge measurements* (Tech. Rep. No. 92–144). U.S. Geological Survey.
- Saulnier, G.-M., Obled, C., & Beven, K. (1997). Analytical compensation between DTM grid resolution and effective values of saturated hydraulic conductivity within the TOPMODEL framework. *Hydrological Processes*, 11(9), 1331–1346. doi: 10.1002/(SICI)1099-1085(199707)11:9<1331::AID-HYP563>3.0.CO;2-9

- Schenk, H. J. (2008). The Shallowest Possible Water Extraction Profile: A Null Model for Global Root Distributions. *Vadose Zone Journal*, 7(3), 1119–1124. doi: 10.2136/vzj2007.0119
- Schmadel, N. M., Neilson, B. T., & Stevens, D. K. (2010, November). Approaches to estimate uncertainty in longitudinal channel water balances. *Journal of Hydrology*, 394(3), 357–369. doi: 10.1016/j.jhydrol.2010.09.011
- Staff, S. S., & Natural Resources Conservation Service, United States Department of Agriculture. (2023). *Web Soil Survey*. <https://websoilsurvey.sc.egov.usda.gov/App/WebSoilSurvey.aspx>.
- St. Clair, J., Moon, S., Holbrook, W. S., Perron, J. T., Riebe, C. S., Martel, S. J., ... De Richter, D. B. (2015). Geophysical imaging reveals topographic stress control of bedrock weathering. *Science*, 350(6260), 534–538. doi: 10.1126/science.aab2210
- Theodoratos, N., Seybold, H., & Kirchner, J. W. (2018). Scaling and similarity of a stream-power incision and linear diffusion landscape evolution model. *Earth Surface Dynamics*, 6(3), 779–808. doi: 10.5194/esurf-6-779-2018
- Tolorza, V., Carretier, S., Andermann, C., Ortega-Culaciati, F., Pinto, L., & Mardones, M. (2014). Contrasting mountain and piedmont dynamics of sediment discharge associated with groundwater storage variation in the Biobío River. *Journal of Geophysical Research: Earth Surface*, 119(12), 2730–2753. doi: 10.1002/2014JF003105
- Troch, P. A., Lahmers, T., Meira, A., Mukherjee, R., Pedersen, J. W., Roy, T., & Valdes-Pineda, R. (2015). Catchment coevolution: A useful framework for improving predictions of hydrological change? *Water Resources Research*, 51(7), 4903–4922. doi: 10.1002/2015WR017032
- Wu, S., Zhao, J., Wang, H., & Sivapalan, M. (2021). Regional Patterns and Physical Controls of Streamflow Generation Across the Conterminous United States. *Water Resources Research*, 57(6), e2020WR028086. doi: 10.1029/2020WR028086
- Yoshida, T., & Troch, P. A. (2016). Coevolution of volcanic catchments in Japan. *Hydrology and Earth System Sciences*, 20(3), 1133–1150. doi: 10.5194/hess-20-1133-2016
- Zavala, V., Carretier, S., & Bonnet, S. (2020). Influence of orographic precipitation on the topographic and erosional evolution of mountain ranges. *Basin Research*, 32(6), 1574–1599. (Publisher: European Association of Geoscientists & Engineers) doi: 10.1111/bre.12443
- Zhang, W., & Montgomery, D. R. (1994). Digital elevation model grid size, landscape representation, and hydrologic simulations. *Water Resources Research*, 30(4), 1019–1028. doi: 10.1029/93WR03553